Mechanisms of HIV-induced peripheral neuropathic pain by focusing on Schwann cell-macrophage interaction

2021

Mpumelelo Ntogwa

Table of Contents

Preface …….. 1

Chapter 1: The role of macrophage-mediated neuroinflammation in the HIV DSN pathogenesis by using X4 gp120-induced neuropathic pain mouse model

Introduction…….. 4

Materials and Methods……. 5

Results……9

Discussion……16

Chapter 2: The regulators of X4-gp120 induced macrophage recruitment to peripheral nerves

Introduction…… 18

Materials and Methods……... 19

Results…… 26

Discussion…….. 35

Summary …… 38

Acknowledgements…… 40

List of Publications…… 41

References……... 42

Preface

Distal sensory neuropathy (DSN) is a hallmark of human immunodeficiency virus (HIV) infection that affects as many as 50% of all individuals infected with HIV and can cause persistent and disabling pain (1). Defining symptoms of DSN include spontaneous/evoked pain, paresthesia, gait instability and autonomic dysfunction (2). Because the mechanisms underlying HIV DSN pathogenesis remain incompletely understood, currently available treatment options are largely unsatisfactory (3).

Pathologically, HIV DSN is characterized by 'dying back' sensory axonopathy and loss of dorsal root ganglion (DRG) neurons (2). Direct neurotoxicity through infection of neurons with HIV has been thought to cause HIV DSN (4). However, it remains controversial whether HIV can infect neurons to locally modulate neurotoxicity, as neurons do not express its main receptor, CD4 (5,6). Alternatively, it is widely accepted that direct interaction of the HIV-1 coat protein glycoprotein120 (gp120) with the primary sensory neurons, which occurs via C-C chemokine receptor type 5 (CCR5) and/or C-X-C chemokine receptor type 4 (CXCR4) chemokine receptors, is a primary causative factor in neural toxicity and HIV DSN pathogenesis (7,8).

HIV strains are subdivided into two major groups based on their cellular tropism: the macrophage-tropic R5 strain and the T-cell line tropic X4 strain (9,10). The R5 HIV-1 strain, which presents persistently during AIDS progression, infects monocytes/macrophages and T-lymphocytes via CCR5 (9,10). Furthermore, R5 HIV-1 gp120 induces macrophage infiltration into the primary sensory neurons of rats, which is mediated by CCR5 expressed on macrophages (5,12). By contrast, the X4 HIV-1 strain, which usually arises only later in the course of infection, preferentially infects T lymphocytes and T-cell lines via CXCR4 but not monocytes/macrophages (9,10). Nonetheless, similar to the R5 strain, perineural application of X4 HIV-1 gp120 induces macrophage infiltration into primary sensory neurons (13). However, there is no convincing evidence demonstrating the mechanisms that underlie T-cell line tropic X4 gp120-induced macrophage infiltration in the peripheral nervous system or its association with HIV DSN pathogenesis. To address this issue I focused on Schwann cells, the peripheral glial cells known to regulate immune cell infiltration and neuroinflammation after nerve injury (14,15).

In chapter one, I investigated the role of macrophages in pain-like behaviors in X4 gp120-induced HIV DSN mouse model. Perineural application of gp120 IIIB or MN induced mechanical hypersensitivity in the ipsilateral hindpaw 7-28 days after the application. Likewise, perineural application of gp120 IIIB elicited spontaneous pain-like behaviors (flinching, scratching, biting and licking) against the ipsilateral hindpaw 7 days after application. Flow cytometry and immunohistochemical analysis studies revealed increased infiltration of bone marrow derived macrophages into the parenchyma of the ipsilateral sciatic nerves and dorsal root ganglia (DRG) 7 days after gp120 IIIB or MN application. I further confirmed that the infiltration of macrophages into the peripheral nerves is associated with the development of X4 gp120-induced pain-like behaviors.

In chapter two, I investigated roles of Schwann cell-derived CXCL1 in X4 HIV gp120-induced macrophage infiltration and pain-like behaviors. I found that CXCL1, a chemoattractant of macrophages and neutrophils was upregulated in primary cultured Schwann cells and mouse sciatic nerve after gp120 IIIB or MN treatment. In subsequent experiments, I showed for the first time that Schwann cell-derived CXCL1, secreted in response to X4 gp120 exposure, was responsible for macrophage infiltration into peripheral nerves and is thereby associated with pain-like behaviors in mice.

The results are described in detail below.

Abbreviations

ANOVA	Analysis of variance
BM	Bone marrow
CCR5	C-C chemokine receptor type 5
CD4	Cluster of differentiation 4
CD11b	Cluster of differentiation 11b
CD31	Cluster of differentiation 31
CD86	Cluster of differentiation 86
CD206	Cluster of differentiation 206
cDNA	Complementary deoxyribonucleic acid
CXCL1	C-X-C chemokine ligand 1
CXCL2	C-X-C chemokine ligand 2
CXCR4	C-X-C chemokine receptor type 4
DMSO	Dimethyl sulfoxide
DRG	Dorsal root ganglia
DSN	Distal sensory neuropathy
GAPDH	Glyceraldehyde 3-phosphate dehydrogenase
GFP	Green fluorescent protein
Gp120	Glycoprotein 120
HIV	Human Immunodeficiency Virus
Iba1	Ionized calcium binding adapter molecule 1
IL	Interleukin
i.p	Intraperitoneal(ly)
IR	Immunoreactivity
IRF	Interferon regulatory factor
MAP2	Microtubule-associated protein-2
MBP	Myelin basic protein
MTT	3-(4,5-dimethyldiazol-2-yl)-2,5-diphenyltetrazolium bromide
PB	Phosphate buffer
PBS	Phosphate buffer saline
PCR	Polymerase chain reaction
rCXCL1	Recombinant C-X-C chemokine ligand 1
RNA	Ribonucleic acid
RSA	Rat serum albumin
RT-PCR	Reverse transcription-polymerase chain reaction
TNFα	Tumor necrosis factor-α

Chapter 1: The role of macrophage-mediated neuroinflammation in the HIV DSN pathogenesis by using X4 gp120-induced neuropathic pain mouse model

Introduction

The exact mechanism underlying HIV DSN pain pathogenesis remains elusive. Sensory peripheral nerves have been suggested to play a role in the pathogenesis of HIV DSN, however there is no convincing evidence to suggest that they are direct targets of HIV infection. HIV is known to target and infect cells of monocyte/macrophage lineage and $CD4^+$ T cells (9,11). Furthermore, virus attachment requires an interaction of the HIV viral envelope protein gp120 with specific host cell expressed CD4 receptors and members of the chemokine receptor family CCR5 and/or CXCR4. CD4 is expressed on the surface of T lymphocytes, macrophages, dendritic cells and brain microglia that are in addition, the main target cells for HIV infection. However, neurons do not express the CD4 receptor required for viral entry (5) thus making direct neurotoxicity from HIV an unlikely mechanism underlying HIV DSN.

Alternatively, the knowledge that HIV-1 viral envelope protein gp120 maintains agonist abilities at CD4 and chemokine receptors, both when virion bound and free-floating as a monomeric protein, has attracted considerable attention for its role in the pathogenesis of HIV DSN. Furthermore, even in the absence of CD4, certain cell types expressing chemokine coreceptors CCR5 and CXCR4 such as neurons remain a target for gp120 binding from both virion associated and monomeric free-floating gp120 leading to the activation of these receptors and induction of signaling pathways distinct to HIV infection (16,17).

In vivo models of HIV DSN represent the closest system to the clinical setting while still allowing researchers the ability to manipulate specific parameters. In the mouse model, the use of gp120 has allowed the mirroring of HIV DSN-associated pathological changes observed in humans (18). Established *in vivo* models utilizing different delivery mechanisms such as perineural, intrathecal or transgenic all have demonstrated nerve toxicity accompanied by pain like behaviors. This has given enough precedence to allow neurotoxicity and hypersensitivity following gp120 exposure to become widely accepted.

It is well established that nerve injury results in the infiltration of immune cells such as macrophages and the local release of multiple mediators and is associated with neuropathic pain. In the case of HIV DSN, many studies report macrophage infiltration at sites of pathology (19-21). Consistent with clinical findings, the administration of HIV-1 gp120 has been shown to induce macrophage infiltration into the primary sensory neurons of rats (5,12,13). Nevertheless, the comprehensive role of macrophages in the pathogenesis of HIV DSN has not been clearly established. To address this issue, I examined the involvement of macrophage-mediated neuroinflammation in the HIV DSN pathogenesis by using X4 gp120-induced neuropathic pain mouse model.

In this chapter, I generated an HIV DSN mouse model capable of recapitulating HIV-DSN symptoms observed in humans. I show that recombinant X4 HIV-1 gp120 directly delivered to the mouse sciatic nerve induced both mechanical hypersensitivity and spontaneous pain-like behaviors, and that infiltration of macrophages into the peripheral nerves is associated with the development of pain-like behaviors.

Materials and Methods

Animals

All experiments were performed according to the ethical guidelines of the Kyoto University Animal Research Committee (approval number: 17–57). All efforts were made to minimize the number of animals used and to limit experimentation to necessary studies. Pregnant Wistar/ST rats and male C57BL/6J JmsSlc mice (5–7 weeks) were purchased from Japan SLC (Shizuoka, Japan). C57BL/6-Tg (CAG-EGFP) transgenic mice (GFP-transgenic mice) were purchased from Japan SLC and maintained in-house. All animals were housed under a 12 h light–dark cycle at a constant ambient temperature (24 ± 1°C) and humidity (55 ± 10%), and were allowed access to food and water ad libitum.

Reagents

Recombinant X4 HIV-1 gp120 IIIB (>95% pure; Immunodiagnostics, Woburn, MA) and gp120 MN (>90% pure; Prospec-Tany Technogene, Ness-Ziona, Israel) were diluted in rat serum albumin (RSA; Sigma-Aldrich, St. Louis, MO) at a concentration of 1.6 ng/μL (13 nM) or in appropriate culture medium at a concentration of 5 nM prior to use for *in vivo* (21) and in vitro assays (22), respectively. Clodronate liposomes, which depletes systemic macrophages, and control liposomes (Clophosome®-N; FormuMax Scientific, Sunnyvale, CA) were used without dilution.

Pain models

For the mouse model of HIV DSN, surgery was performed as previously described (13). Under 50 mg/kg intraperitoneal sodium pentobarbital (Nacalai Tesque) anesthesia and aseptic conditions, the right sciatic nerve was exposed in the popliteal fossa without damaging the perineurium. A 3 x 2 mm gel foam, Oxidised Regenerated Cellulose (ORC) (Surgicel®; Ethicon US, Somerville, NJ), was briefly soaked until saturation in 250 μL saline containing either 0.1% RSA, 13 nM gp120 IIIB, or 13 nM gp120 MN. The ORC was then wrapped loosely around the sciatic nerve 2–3mm proximal, so as to avoid nerve constriction. The nerve was gently manipulated back into place and the muscle and skin incisions were closed with 3/0 sutures (Natsume Seisakusho, Tokyo, Japan).

Behavioral testing

Behavioral testing was conducted to measure mechanical hypersensitivity and spontaneous pain behaviors at various time points after perineural application of gp120 or vehicle. All behavioral tests were conducted by the same investigator, who was blinded to the treatment group of each animal.

von Frey filament test. Mechanical sensitivity was assessed by measuring the paw withdrawal threshold using calibrated von Frey filaments (Touch test®; North Coast Medical, Morgan Hill, CA) as previously described with slight modifications (24,25). One day prior to testing as well as on every behavioral testing day, mice were acclimatized on a metal mesh floor in small Plexiglas cubicles (length, 9 cm; width, 5 cm; height, 5 cm) for 1 h. Mechanical sensitivity was measured using a set of seven calibrated von Frey filaments of increasing strength (0.008, 0.02, 0.04, 0,07, 0.16, 0.4, and 1 g) applied to the plantar surface of the right hind paw until the filament bent slightly for a few seconds. A positive or negative response was defined as a paw withdrawal response from the pressure of a filament or lack of a response within 6 sec, respectively. The 0.16 g force filament was applied first. If a positive response to a given filament occurred, the next smaller filament was applied. If a negative response occurred, the next higher filament was applied. The test was continued until four responses were collected after the first change in response, and the 50% paw withdrawal threshold was then converted to the cutaneous nociceptive threshold using an adaptation of the Dixon up-down paradigm (25). The behavioral test was performed on the indicated days as per the experiment requirements.

Spontaneous pain behaviors. Mice were acclimatized to dim light (approximately 20 lux) for more than 20 min and then placed inside the test chamber (diameter, 11 cm; height, 18 cm). The test chamber was set to dim light and constant room temperature (24 ± 1°C). Three behavioral signs thought to represent different components of spontaneous pain behavior were assessed, including flinching, scratching (severe flinching), and biting/licking of the operated hind paw (26). After a 30 min acclimatization period, these behavioral signs were recorded for 60 min using a digital video camera (Logical® HD Webcam C615; logicol, Tokyo, Japan), which was positioned in front of the animal to capture all limb movements within the camera angle. The recording was later visually examined to evaluate the frequency and duration of aberrant asymmetrical limb movements. Observation of the recording was conducted instead of real-time observation to avoid possible confounding influences of human signaling on animal behavior.

Generation of GFP-positive bone marrow (BM)-chimeric mice

BM transplantation was carried out as previously reported (27-29) with slight modifications. BM recipients were male 6-week-old C57BL/6J mice. Recipient mice received 8 Gy total body irradiation for 9 min. GFP-positive BM cells were obtained from the femurs of euthanized donor GFP transgenic mice. Femur-derived GFP-positive BM cells were placed into a microtube and suspended in sterile PBS after centrifugation at 1,800 rpm for 10 min. About 3–5 h after irradiation, recipient mice were transplanted with 2.0×10^6 GFP-positive BM cells by intravenous tail vein injection. Before using GFP-

positive BM chimeric mice, I confirmed that these mice could survive under specific pathogen-free conditions for more than 6 weeks, even after substitution of peripheral immune cells with donor mice derived BM cells. In addition, I confirmed that abnormal findings were not present in the surviving mice, suggesting the reliability of my BM experiment results. At 6 weeks after GFP-positive BM cell transplantation, all chimeric mice were subjected to experiments at 12 weeks of age. Flow cytometry was used to confirm the complete substitution of BM-derived cells by GFP-positive BM-derived cells.

Immunohistochemistry in mouse sciatic nerve and DRG sections

After perineural application of gp120 or vehicle, mice were deeply anesthetized with sodium pentobarbital (50 mg/kg, i.p.) and intracardially perfused with freshly prepared 4% paraformaldehyde in 0.1 M phosphate buffer (PB). After perfusion, the bilateral sciatic nerves and fourth lumbar vertebrae (L4) DRGs were quickly removed. All tissues were post-fixed in 4% paraformaldehyde for 4 h and then transferred to 15% sucrose (Nacalai Tesque) solution in 0.1 M PB for 24 h at 4°C. All tissues were then frozen in embedding compound (Sakura Finetek, Torrance, CA). Frozen sections (16 μm) were cut with a cryostat (Leica CM 1850; Leica Microsystems, Wetzlar, Germany) and thaw-mounted on MAS-coated glass slides (Matsunami Glass, Osaka, Japan). The sections were then blocked in blocking buffer (PBS containing 0.1% Tween 20 and 5% normal goat serum; Vector Laboratories) for 1 h at room temperature and subsequently incubated for 24 h at 4°C with the following primary antibodies: rabbit anti-Iba1 (1:500; Wako Pure Chemical Industries, Osaka, Japan), rat anti-Gr-1/Ly-6G antibody (1:200; R&D Systems) or rat anti-CD31 antibody (1:100; Becton, Dickinson and Company, Franklin Lakes, NJ). The antibodies were washed three times with PBS and incubated for 1.5 h at room temperature with the appropriate secondary antibodies conjugated to Alexa Fluor™ 488 and/or 594 (1:200). The slides were then cover-slipped with Vectashield (Vector Laboratories). All images were acquired using a laser scanning confocal microscope (Fluoview FV10i Confocal Microscope, Olympus, Tokyo, Japan). Next, 6–9 fields (2–3 fields x three independent samples) were selected randomly from each group, and the numbers of immunolabeled cells were counted. An area of each sample section was analyzed using a computer-assisted system (ImageJ software; National Institute of Mental Health, Bethesda, MD). Cell numbers per mm^2 were then calculated.

Flow cytometry assay

GFP-positive cells in the peripheral blood. To identify the purity of GFP-positive cells in the peripheral blood following BM transplantation, 100 μL blood was collected from the tail vein of each chimeric mouse 6 weeks after BM transplantation. The collected blood was dissolved in 300 μL saline and gently mixed for 10 sec to hemolyze erythrocytes. After adding 1 mL saline to restore osmotic pressure, the solution was centrifuged at 2,000 x g for 5 min. After aspirating the supernatant, the pellet was washed with 1 mL saline and centrifuged at 2,000 x g for 5 min. After aspirating the supernatant, the pellet was gently resuspended in 500 μL ice-cold fluorescence activated cell sorting (FACS) buffer (0.02 M

ethylenediaminetetraacetic acid and 0.01% BSA in PBS; Affynetrix, Santa Clara, CA). The population of GFP-positive cells was assessed by FACS (BD FACSAria™ II; Becton, Dickinson and Company, Franklin Lakes, NJ) and FACS Diva software. FACS gating was performed to include all GFP positive cells (approximately 10% of all counted cells) in blood samples from GFP transgenic mice. The same setting for the gating area was applied in subsequent experiments.

Sciatic nerve and DRG macrophages.

Macrophages were prepared from the sciatic nerve and DRG as previously described (Labuz et al., 2009; Liu et al., 2017). Briefly, sciatic nerves and DRGs were placed into the same sample tube and enzymatically digested in PBS containing 0.3 % collagenase (Thermo Fisher Scientific, Waltham, MA) and 0.4 % dispase (Thermo Fisher Scientific) for 45–60 min at 37°C. Cells were then washed with 500 µL PBS and centrifuged at 1,000 x g for 5 min. A Percoll (Sigma-Aldrich) gradient was used to separate monocytes/macrophages from myelin and nerve debris as follows. After aspirating the supernatant, the pellets were resuspended in 600 µL 25% Percoll and centrifuged at 1,000 x g for 5 min. An intermediate layer including the monocyte/lymphocyte/basophil pellicle was moved to a new microtube, washed in 500 µL PBS, and centrifuged at 1,000 x g for 5 min. Cells were incubated with FITC-conjugated anti-mouse CD11b (1:50; BD Biosciences, Systems & Reagents, San Jose, CA) and per CP/Cy5.5 anti-mouse F4/80 (1:50; BioLegend, San Diego, CA) for 1 h at 4°C. Pellets were then washed with 1 mL FACS buffer and centrifuged at 2,000 x g for 5 min. After aspirating the supernatant, the pellets were gently resuspended in 350 µL ice-cold FACS buffer. The population of CD11b/F4/80-double positive cells was assessed by FACS and FACS Diva software. In all FACS analyses, I counted at least 10,000 cells/sample. Compensation and gating were performed using negative, single-stained controls and isotype controls.

Statistical analysis

Data are presented as means ± S.E.M. and were analyzed using GraphPad Prism version 5.0. (GraphPad Software, San Diego, CA). Differences between two groups were compared using a Student's t-test or Mann–Whitney U-test. Data from more than two groups were compared using a one-way or two-way analysis of variance (ANOVA), followed by a Bonferroni's or Tukey's multiple comparisons test. Statistical analyses of the 50% withdrawal thresholds in the von Frey filament test were performed using a Mann–Whitney U-test or Kruskal–Wallis test followed by Dunn's multiple comparison test for each day. In all cases, $p < 0.05$ was considered statistically significant.

Results

Perineural X4 gp120 application induces pain behaviors

I generated the HIV DSN mouse model by topically exposing the right sciatic nerve (ipsilateral) of C57BL/6J mice to oxidized regenerated cellulose after briefly soaking it in either the rat serum albumin (vehicle), X4 strain gp120 IIIB (13nM) or gp120 MN (13nM). Similar to previous reports (13,22,30), perineural application of gp120 IIIB (13 nM) or MN (13 nM) to the sciatic nerve significantly lowered the 50% withdrawal threshold in the ipsilateral hindpaw 7–21 days after the application, compared with vehicle-treated mice (Fig. 1-1A). The decreased 50% withdrawal threshold was gradually recovered to the same level observed in vehicle-treated mice by 28 days after the application. Likewise, perineural application of gp120 IIIB evoked spontaneous pain behaviors (flinching, scratching, biting and licking) against the ipsilateral hindpaw, while there were no pain behaviors against the contralateral hindpaw. The duration of spontaneous pain behaviors in 60-min observation period was significantly increased 7 days after gp120 IIIB application, compared with those in vehicle-treated mice (Fig. 1-1B).

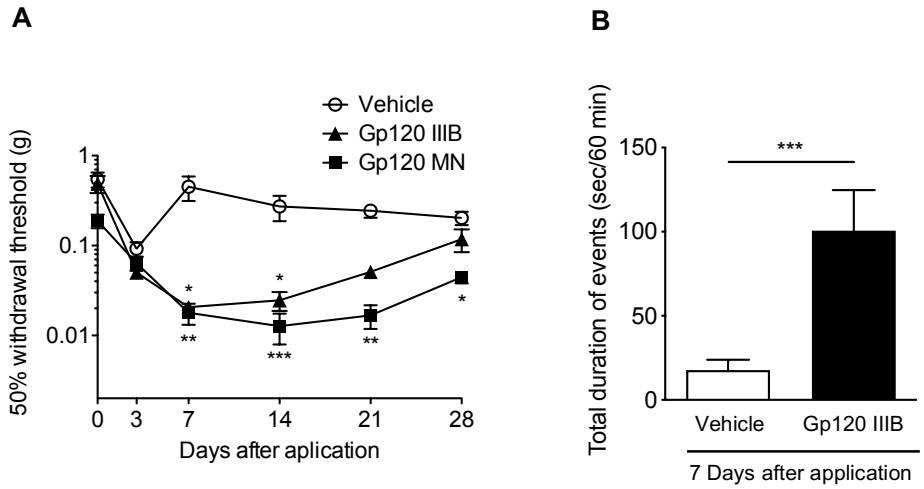

Fig. 1-1. Pain-like behaviors after perineural X4 gp120 application in mice. Gp120 IIIB (13 nM), gp120 MN (13 nM) or vehicle (0.1% RSA) was perineurally applied to the sciatic nerve on day 0. Each behavioral test in the ipsilateral hindpaw was performed on the indicated days. **(A)** Time-course changes in 50% withdrawal threshold (g) in response to mechanical stimuli in the ipsilateral hindpaw. Paw withdrawal thresholds were assessed by using von Frey filaments just before gp120 application (day 0) or 3, 7, 14, 21 and 28 days after X4 gp120 application. n = 4–8. *p < 0.05, **p < 0.01, ***p < 0.001 vs. vehicle-treated mice (Dunn's multiple comparisons test following Kruskal-Wallis test on each day). **(B)** Spontaneous pain-like behaviors 7 days after gp120 IIIB treatment. Total duration (sec) showing flinching, scratching and biting/licking in the ipsilateral hindpaw was measured during a 60 min observation period. n = 9. ***p < 0.001 (Mann–Whitney U test). Each point or column represents the mean ± S.E.M.

Perineural X4 gp120 application induced macrophage infiltration into the sciatic nerve and DRG

Recently, it has been reported that macrophage accumulation around the peripheral nerve is observed in patients with HIV DSN (2). In line with this, I assessed the infiltration of macrophages into the sciatic nerves and DRGs of gp120-treated mice. Perineural application of gp120 IIIB or MN to the sciatic nerve increased Iba1-immunoractivity (IR) in the ipsilateral side of both the sciatic nerve and DRG 7

days after application (Fig. 1-2A). The number of Iba1-labeled macrophages in the sciatic nerve 7 days after gp120 IIIB application increased nearly ten-fold compared to vehicle-treated mice. This was more drastic than the change 3 days after gp120 application (Fig. 1-2C). Likewise, the number of Gr1-IR neutrophils significantly increased by 2–3 times in the sciatic nerve both 3 and 7 days after gp120 application (Fig. 1-2C). These immunohistochemical data were further confirmed by flow cytometry data demonstrating that the number of F4/80- and CD11b double positive macrophages was significantly increased in the ipsilateral sciatic nerve and DRG after gp120 IIIB or gp120 MN application compared with the vehicle-treated group (Fig. 1-3).

To further confirm the infiltration of macrophages, I used BM chimeric mice derived by transferring donor BM cells from GFP-transgenic mice to recipient C57BL/6J mice. Reconstitution of GFP-positive BM chimeric mice resulted in 98.3% of peripheral blood cells in recipient mice being replaced by donor GFP-positive cells 6 weeks after transplantation (Fig. 1-4). In the ipsilateral sciatic nerve and DRG of vehicle-treated GFP-positive BM chimeric mice, a small number of GFP negative/Iba1-positive cells (representing resident macrophages) and GFP/Iba1-double positive cells (representing infiltrated macrophages) were observed 7 days after perineural application of the vehicle control. By contrast, perineural application of gp120 IIIB or MN significantly increased GFP/Iba1-double positive cells, rather than GFP-negative/Iba1-positive cells (Fig. 1-5B). Furthermore, these increased GFP-positive cells were less co-localized with CD31-positive endothelial cells in gp120-treated mice, while macrophages were mainly detected along CD31-positive endothelial cells in vehicle-treated mice (Fig. 1-6) indicated by the arrow head as macrophages in the circulating blood), suggesting infiltration of macrophages into the parenchyma of the sciatic nerve and DRG in mice with perineural gp120 application.

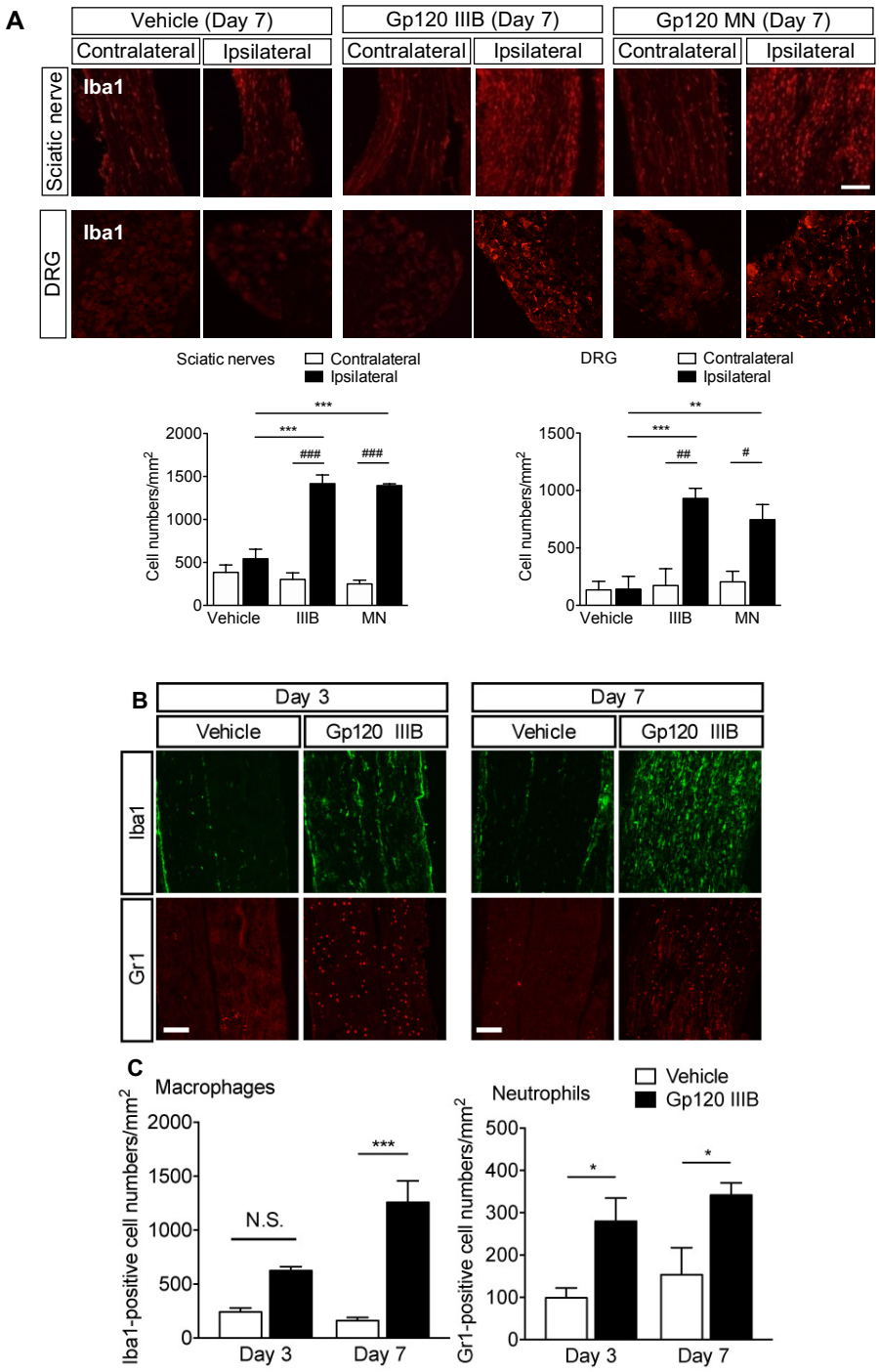

Fig. 1-2. Increased macrophages and neutrophils in the mouse sciatic nerve and dorsal root ganglia (DRG) after perineural X4 gp120 application. Gp120 IIIB (13 nM), gp120 MN (13 nM) or vehicle (0.1% RSA) was perineurally applied to the right side of the sciatic nerve (ipsilateral). At 3 and 7 days after application of gp120 IIIB (13 nM), gp120 MN (13 nM) or vehicle (0.1% RSA), mice were subjected to immunohistochemistry. **(A)** Representative confocal microscopy images showing Iba1-immunoreactivity (IR) in the longitudinal sections of the mouse sciatic nerve (upper panels) and DRG (lower panels) 7 days after the X4 gp120 application. Scale bar = 100 μm. The lower graphs show the quantitative analyses for the number of Iba1-labeled cells (macrophages) per mm2. Each column represents the mean ± S.E.M. n=3. **p < 0.01, ***p < 0.001, #p < 0.05, ##p < 0.01, ###p < 0.001 (Bonferroni's multiple comparisons test following two-way ANOVA). **(B)** Representative confocal microscopy images illustrating Iba1 (green)- and Gr1 (red)-immunoreactivity in the ipsilateral sciatic nerve. Scale bar = 100 μm. (**C**) Number of Iba1-labeled cells (macrophages) and Gr1-labeled cells (neutrophils) per mm^2 in the mouse ipsilateral sciatic nerve. Each column represents the mean ± S.E.M. n = 3. *p < 0.05, ***p < 0.001 (Bonferroni's multiple comparisons test following two-way ANOVA). N.S.: not significant.

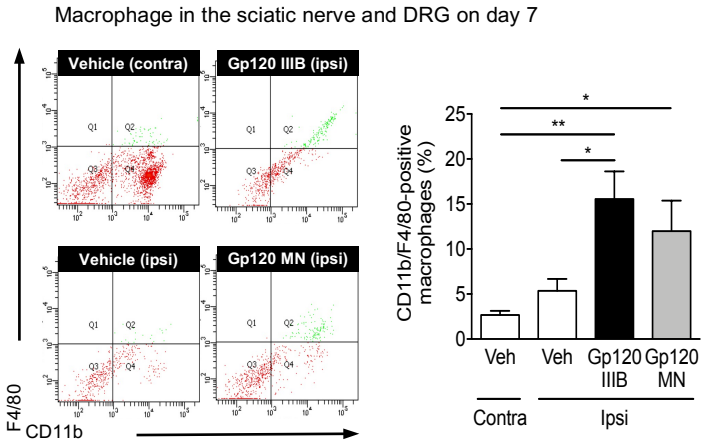

Fig. 1-3. Representative flow cytometric analysis of macrophages expressing F4/80 and/or CD11b surface markers in cell suspensions isolated from the contralateral or ipsilateral side of the sciatic nerve and DRG 7 days after X4 gp120 application. The F4/80- and CD11b-double positive cell population (green colored) was identified as macrophages. The right panel shows the percentage of F4/80- and CD11b-double positive macrophage in 10,000 cells isolated from the sciatic nerve and DRG. Each column represents the mean ± S.E.M. n = 5–7. *p < 0.05, **p < 0.01 (Bonferroni multiple comparisons test following one-way ANOVA)

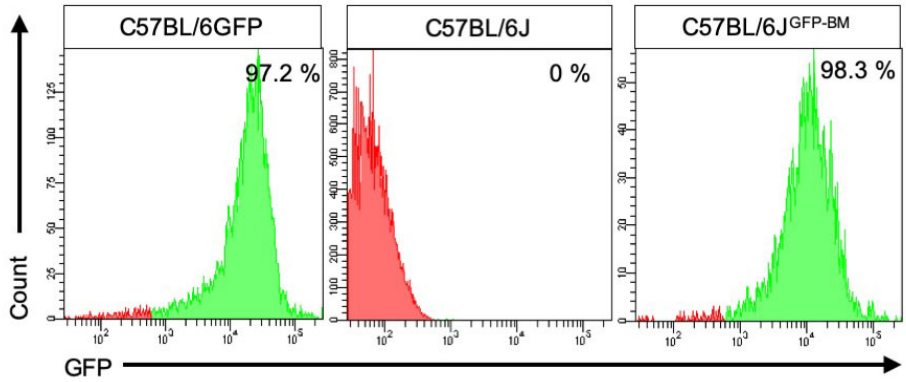

Fig. 1-4 Representative histogram of peripheral blood GFP-positive cells in BM chimeric mice generated by adoptive transfer of donor GFP-transgenic BM cells into recipient C57BL/6J mice. Flow cytometry analysis was conducted using peripheral blood collected from each chimeric mouse. Red and green peaks illustrate the populations of GFP-negative and GFP-positive cells, respectively. BM-derived cells from wild-type mice were used as GFP-negative controls, and BM-derived cells derived from GFP-transgenic mice were used as GFP-positive controls, respectively. Flow cytometry analysis revealed that 98.3% of BM-derived recipient cells were replaced with GFP-positive donor cells.

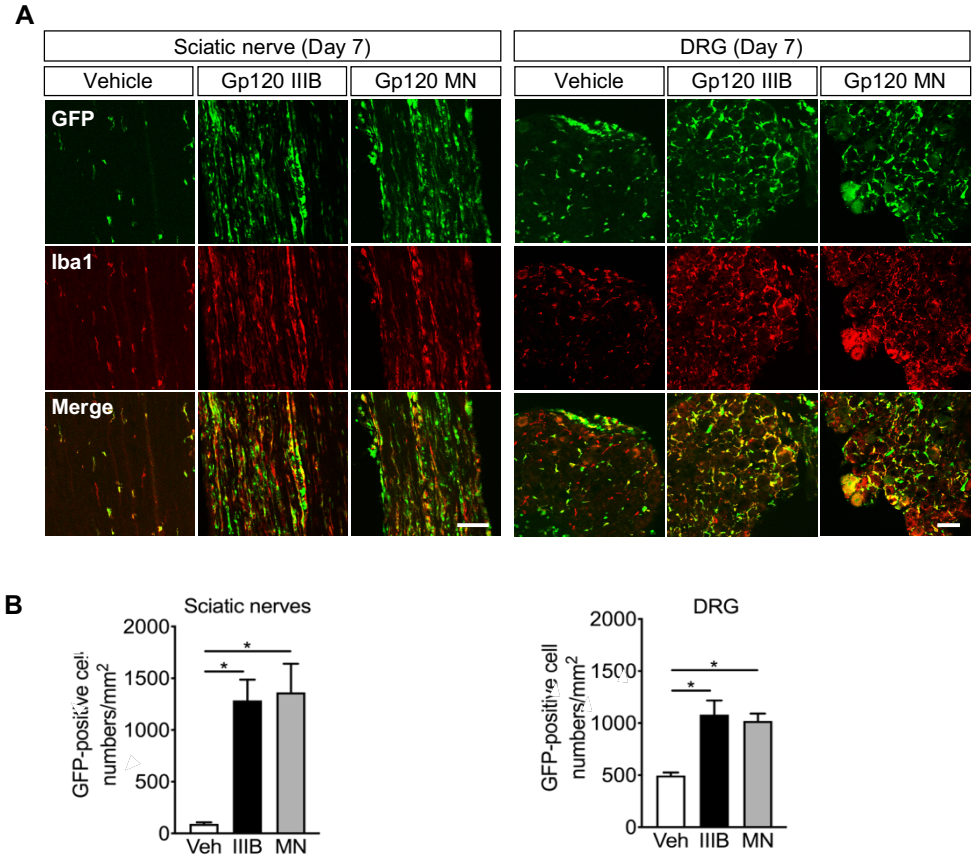

Fig. 1-5. Macrophage infiltration into the mouse sciatic nerve and dorsal root ganglia (DRG) after perineural X4 gp120 application. Gp120 IIIB (13 nM), gp120 MN (13 nM) or vehicle (0.1% RSA) was perineurally applied to the sciatic nerve. **(A)** Representative confocal microscopy images for GFP fluorescence (green) and Iba1-IR (red) in the ipsilateral sciatic nerve and DRG of GFP+ bone marrow (BM) chimeric mice 7 days after X4 gp120 application. Scale bar= 100 μm. **(B)** The graphs show the quantitative analyses for the number of GFP-positive cells per mm2. n =3. *p < 0.05 (Bonferroni's multiple comparisons test following two-way ANOVA). Each column represents the mean ± S.E.M.

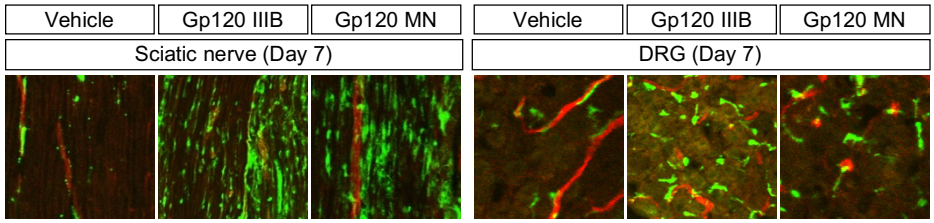

Fig. 1-6. Macrophage infiltration into the parenchyma of the sciatic nerve and dorsal root ganglia (DRG) after perineural X4 gp120 application. Representative confocal microscopy images for GFP fluorescence (green) and endothelial cell marker CD31-IR (red) in the ipsilateral sciatic nerve and DRG of GFP+ bone marrow (BM) chimeric mice 7 days after X4 gp120 application. Scale bar =100 μm.

Macrophage depletion abolished X4 gp120-induced pain behaviors

The effects of clodronate liposomes, a well-characterized macrophage depleting compound (31), on X4 gp120-induced pain behaviors were investigated. As indicated by the timeline in Figure 1-7A, clodronate liposomes or control liposomes were injected intraperitoneally three times. Flow cytometry revealed that a considerable proportion of F4/80- and CD11b-double positive macrophages in the ipsilateral sciatic nerve and DRG 7 days after gp120 IIIB treatment were significantly decreased, with similar levels to that of vehicle-treated mice (Fig.1-7B). Consistent with the flow cytometry data, immunohistochemical studies demonstrated that clodronate treatment markedly decreased Iba1-IR cells on the ipsilateral sciatic nerve and DRG in gp120 IIIB-treated mice (Fig. 1-7C). Under these conditions, treatment with clodronate liposomes significantly inhibited gp120-induced mechanical hypersensitivity (Fig. 1-7D) and spontaneous pain behaviors (Fig. 1-7E) 7 days after gp120 IIIB application.

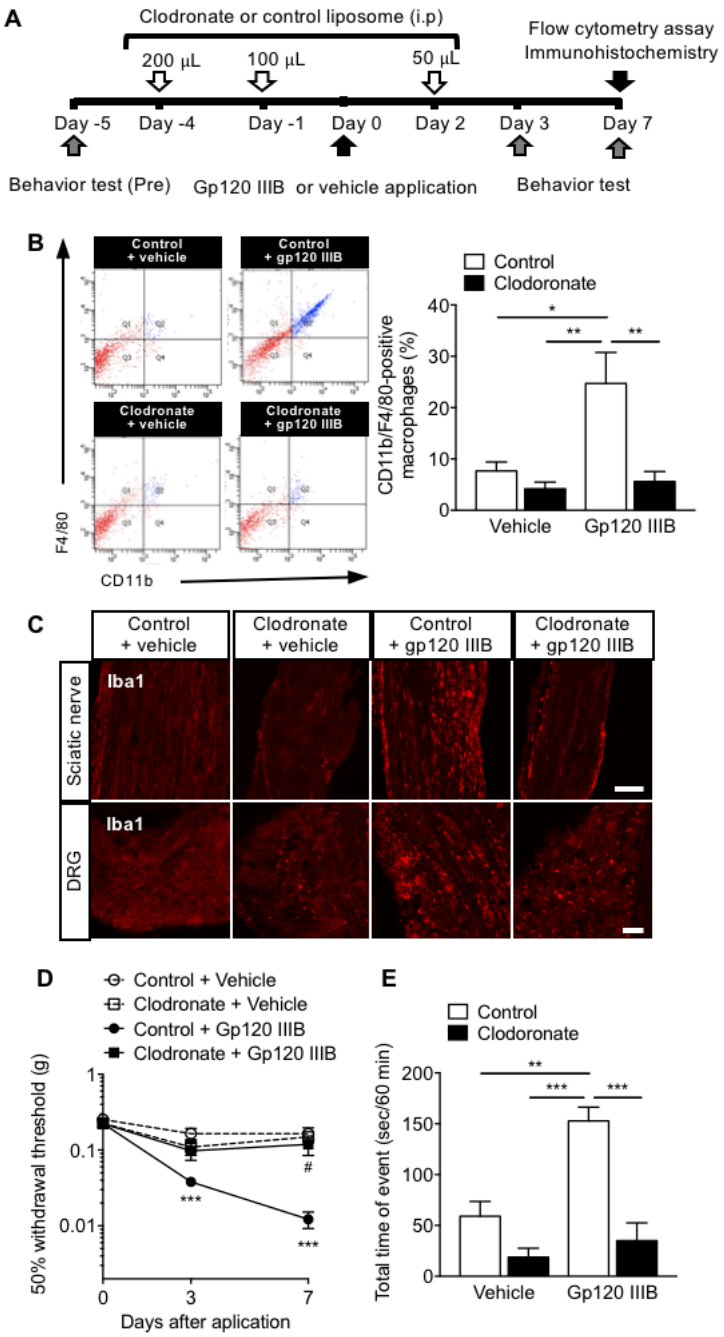

Fig. 1-7. Effects of clodronate macrophage depletion on gp120 IIIB-induced painlike behaviors. Clodronate or control liposomes were injected intraperitoneally before and after gp120 IIIB (13 nM) or vehicle (0.1% RSA) administration. (**A**) Timeline of experiments investigating the effects of clodronate liposomes on gp120 IIIB-induced infiltration of macrophages and pain-like behaviors. (**B**) Representative flow cytometric analysis of macrophages expressing F4/80 and/ or CD11b surface markers in cell suspensions isolated from the ipsilateral sciatic nerve and dorsal root ganglia (DRG). F4/80- and CD11b-double positive cell population (blue colored) was identified as macrophages. The right panel shows the percentage of F4/80- and CD11b-double positive macrophages in 10,000 cells obtained from the sciatic nerve and DRG. n = 4–5. *p < 0.05, **p < 0.01 (Bonferroni's multiple comparisons test following two-way ANOVA). (**C**) Representative confocal microscopy images illustrating Iba1-immunoreactivity in the ipsilateral sciatic nerve and DRG 7 days after gp120 IIIB application in clodronate or control liposome-treated mice. Scale bar = 100 μm. (**D**) Gp120 IIIB-induced mechanical hypersensitivity. Paw withdrawal thresholds were assessed using von Frey filaments just before application (day 0) and on days 3 and 7 after gp120 IIIB application in clodronate or control liposome-treated mice. n = 3–4. ***p < 0.01 vs. control liposome + vehicle-treated group. #p < 0.05 vs. control liposome + gp120 IIIB treated group (Dunn's multiple comparisons test following a Kruskal–Wallis test on each day). (**E**)

Spontaneous pain-like behaviors (flinching, scratching, and biting/licking) during a 60 min observation period 7 days after gp120 IIIB application in clodronate or control liposome-treated mice. n = 3–4. **p < 0.01, ***p < 0.001 (Bonferroni's multiple comparisons test following two-way ANOVA). Each column or point represents the mean ± S.E.M.

Discussion

Here, I generated an X4 HIV DSN mouse model to provide some insight into the role of macrophage-mediated neuroinflammation in the HIV DSN pathogenesis.

Whilst the exact pathogenesis of HIV DSN is unclear, HIV DSN is hypothesized to result, not by direct infection to neurons, as neurons are believed not to express CD4 receptors required for cell entry of HIV, but rather via interaction of the HIV envelope glycoprotein, gp120, with neuronally expressed chemokine receptors, CXCR4 and CCR5. Virus-bound gp120 is essential for initiating HIV-host cell binding but monomeric gp120 also maintains the ability to target, bind and activate certain cell types expressing chemokine receptor CCR5 or CXCR4. Therefore, the occurrence of free-floating monomeric gp120 has given researchers the rationale to use recombinant monomeric gp120, in the absence of HIV virions to attempt to investigate neuropathic pain mechanisms underlying HIV DSN.

Chronic pain is a common phenotype that accompanies HIV patients with HIV DSN (2). Numerous studies now provide consistent data demonstrating the induction of hypersensitivity behavior in animals exposed to HIV-1 gp120 (18). Consistent with these studies, my findings show that recombinant X4 HIV-1 gp120 delivered directly to the mouse sciatic nerve induced mechanical hypersensitivity that persisted for weeks. Although representative of symptoms encountered in HIV DSN patients, spontaneous pain has rarely been reported in animal models of HIV DSN. Consistent with a previous report (32), I found the consistent presence of spontaneous pain-like behaviors in the HIV DSN mouse model. Together, these findings suggest that the gp120 HIV DSN model, at least in part, represents a relevant approach to the translation from preclinical finding to patients with painful HIV DSN.

It is well established that nerve injury and Wallerian degeneration result in the infiltration of macrophages and local release of multiple mediators. In the case of HIV, HIV DSN severity is highly correlated with the degree of inflammatory cell infiltration indicating macrophages to be potential mediators (33,34). One of the most consistent pathologies in the DRG appears to be the activation of inflammatory mechanisms that leads to the injury of DRG neurons. Furthermore, the presence of proinflammatory cytokines, such as TNF-α as well as other mediators of inflammation is consistently demonstrated in the DRG of HIV patients (35,36) and together, in patients with HIV DSN, these pathological processes manifest as painful sensory neuropathy. Consistently, utilizing the HIV DSN mouse model, I confirmed that perineural application of gp120 from both HIV IIIB and MN strains, but not heat-inactivated gp120 IIIB, increased macrophage infiltration into the parenchyma of ipsilateral sciatic nerve and DRG, which correlated with the appearance of mechanical hypersensitivity and spontaneous pain-like behaviors in only the ipsilateral side.

There is a growing interest in understanding the involvement of immune cells in the pathogenesis of neuropathic pain. Among the different approaches that can target macrophages, the most radical is represented by their depletion, commonly obtained by means of clodronate-containing liposome formulation. The depletion of macrophages by the use of clodronate liposomes has been useful to understand their role in the establishment and development of disease. Consistent with previous reports (29,37), depletion of macrophages by clodronate liposomes suppressed gp120 IIIB-induced pain-like behaviors. Taken together, these findings suggest that infiltration of macrophages into the peripheral nerves is associated with the development of X4 gp120-induced pain-like behaviors.

In conclusion, the data presented in this chapter suggest a link between the infiltration of bone marrow stem cell-derived macrophages into the peripheral nerve and the resultant pain-like behaviors following the perineural application of X4 gp120.

Chapter 2: The regulators of X4-gp120 induced macrophage recruitment to peripheral nerves

Introduction

The pathogenesis of HIV DSN is hypothesized to be caused by two cellular mechanisms (38,39). One is thought to be neuronally-mediated in which the HIV viral proteins directly activate CCR5 and/ or CXCR4 chemokine receptors expressed on neurons (38). This leads to the increases in intracellular calcium levels and eventual axonal degeneration, although the pathways linking the activation and axonal degeneration remain obscure. The other mechanism is thought to be initiated indirectly via non-neuronal cells as a result of aberrant cytotoxic immune cell signaling and mediator release (39). It remains to be determined whether one pathway is dominant or in fact synergy of multiple pathways is required.

Different HIV strains specifically target and infect certain cell types via the selectivity of gp120 to one or both of CCR5 or CXCR4 (9,10). The majority of viral strains, especially early on during infection, target CCR5 and are known as either CCR5 (R5)-tropic or M-tropic viruses as they preferentially infect and replicate in macrophages (9,11). Growing evidence suggests that macrophages may play a key role in the pathogenesis of HIV-DSN (19-21). Indeed, infiltrated macrophages were found in the DRG of AIDS patients with a history of HIV DSN. Consistent with clinical findings, the R5 HIV-1 gp120 is shown to induce macrophage infiltration into the primary sensory neurons of rats, which is mediated by CCR5 expressed on macrophages (5,12). Therefore, the macrophage-dependent immune responses leading to neurotoxicity is considered to be one of the causes of pathogenesis of R5 gp120-related neuropathy (5,12). Different from the R5 HIV-1 strain, the X4 HIV-1 strain, which usually arises only later in the course of infection, preferentially infects T lymphocytes and T-cell lines via CXCR4 but not monocytes/macrophages (9,11). As shown in chapter 1, similar to the R5 strain, perineural application of X4 HIV-1 gp120 induces macrophage infiltration into primary sensory neurons . However, how X4 HIV-1 gp120 induces macrophage infiltration and its subsequent association with HIV DSN pathogenesis remains to be elucidated. Therefore further investigation is warranted in the continuing effort to uncover the mechanism underlying HIV DSN.

Schwann cells, the peripheral glial cells, are known to regulate immune cell infiltration and neuroinflammation after nerve injury by producing cytokines, chemokines, and extracellular proteases (14,15). Considering these previous findings, I hypothesized here that Schwann cells contribute to X4 gp120-induced macrophage infiltration in the peripheral nervous system and to the subsequent development of HIV DSN.

In this chapter, I investigated the responsible cell types (especially focusing on Schwann cells) and regulators of X4 gp120-induced macrophage recruitment to peripheral nerves and associated pain-like behaviors. I showed that X4 gp120 had no direct effects on macrophages. Rather, I demonstrated

for the first time that Schwann cells in response to X4 gp120 released the chemoattractant CXCL1 to induce macrophages chemotaxis into peripheral nerve which in turn caused pain-like behaviors.

Materials and Methods

Animals

All experiments were performed according to the ethical guidelines of the Kyoto University Animal Research Committee (approval number: 17–57). All efforts were made to minimize the number of animals used and to limit experimentation to necessary studies. Pregnant Wistar/ST rats and male C57BL/6J JmsSlc mice (5–7 weeks) were purchased from Japan SLC (Shizuoka, Japan). C57BL/6-Tg(CAG-EGFP) transgenic mice (GFP-transgenic mice) were purchased from Japan SLC and maintained in-house. All animals were housed under a 12 h light–dark cycle at a constant ambient temperature (24 ± 1°C) and humidity (55 ± 10%), and were allowed access to food and water ad libitum.

Reagents

Recombinant X4 HIV-1 gp120 IIIB (>95% pure; Immunodiagnostics, Woburn, MA) and gp120 MN (>90% pure; Prospec-Tany Technogene, Ness-Ziona, Israel) were diluted in rat serum albumin (RSA; Sigma-Aldrich, St. Louis, MO) at a concentration of 1.6 ng/μL (13 nM) or in appropriate culture medium at a concentration of 5 nM prior to use for *in vivo* (22) and in vitro assays (23), respectively. Recombinant mouse CXCL1 (rCXCL1; R&D Systems, Minneapolis, MN) was dissolved in sterile bovine serum albumin (Sigma-Aldrich) at a concentration of 12.5 mM. A CXCR2 antagonist, N-(2 bromophenyl)-N'-(2-hydroxy-4-nitrophenyl) urea (SB225002; R&D Systems), was dissolved in dimethyl sulfoxide (DMSO; Nacalai Tesque, Kyoto, Japan) and diluted in phosphate-buffered saline (PBS) prior to injection.

Pain models

For the mouse model of HIV DSN, surgery was performed as previously described (13). Under 50 mg/kg intraperitoneal sodium pentobarbital (Nacalai Tesque) anesthesia and aseptic conditions, the right sciatic nerve was exposed in the popliteal fossa without damaging the perineurium. A 3 x 2 mm gel foam, Oxidised Regenerated Cellulose (ORC) (Surgicel®; Ethicon US, Somerville, NJ), was briefly soaked until saturation in 250 μL saline containing either 0.1% RSA, 13 nM gp120 IIIB, or 13 nM gp120 MN. The ORC was then wrapped loosely around the sciatic nerve 2–3 mm proximal, so as to avoid nerve constriction. The nerve was gently manipulated back into place and the muscle and skin incisions were closed with 3/0 sutures (Natsume Seisakusho, Tokyo, Japan).

For the rCXCL1-evoked pain model, 3 x 2 mm ORC was briefly soaked in solution either containing 50 nM rCXCL1 or 0.1% RSA, and then loosely wrapped around the sciatic nerve, as described above.

Behavioral testing

Behavioral testing was conducted to measure mechanical hypersensitivity and spontaneous pain behaviors at various time points after perineural application of gp120 or vehicle. All behavioral tests were conducted by the same investigator, who was blinded to the treatment group of each animal.

von Frey filament test. Mechanical sensitivity was assessed by measuring the paw withdrawal threshold using calibrated von Frey filaments (Touch test®; North Coast Medical, Morgan Hill, CA) as previously described with slight modifications (24,25). One day prior to testing as well as on every behavioral testing day, mice were acclimatized on a metal mesh floor in small Plexiglas cubicles (length, 9 cm; width, 5 cm; height, 5 cm) for 1 h. Mechanical sensitivity was measured using a set of seven calibrated von Frey filaments of increasing strength (0.008, 0.02, 0.04, 0,07, 0.16, 0.4, and 1 g) applied to the plantar surface of the right hind paw until the filament bent slightly for a few seconds. A positive or negative response was defined as a paw withdrawal response from the pressure of a filament or lack of a response within 6 sec, respectively. The 0.16 g force filament was applied first. If a positive response to a given filament occurred, the next smaller filament was applied. If a negative response occurred, the next higher filament was applied. The test was continued until four responses were collected after the first change in response, and the 50% paw withdrawal threshold was then converted to the cutaneous nociceptive threshold using an adaptation of the Dixon up-down paradigm (25). The behavioral test was performed on the indicated days as per the experiment requirements.

Spontaneous pain behaviors. Mice were acclimatized to dim light (approximately 20 lux) for more than 20 min and then placed inside the test chamber (diameter, 11 cm; height, 18 cm). The test chamber was set to dim light and constant room temperature (24 ± 1°C). Three behavioral signs thought to represent different components of spontaneous pain behavior were assessed, including flinching, scratching (severe flinching), and biting/licking of the operated hind paw (26). After a 30 min acclimatization period, these behavioral signs were recorded for 60 min using a digital video camera (Logical® HD Webcam C615; logicol, Tokyo, Japan), which was positioned in front of the animal to capture all limb movements within the camera angle. The recording was later visually examined to evaluate the frequency and duration of aberrant asymmetrical limb movements. Observation of the recording was conducted instead of real-time observation to avoid possible confounding influences of human signaling on animal behavior.

Immunohistochemistry in mouse sciatic nerve and DRG sections

After perineural application of gp120 or vehicle, mice were deeply anesthetized with sodium pentobarbital (50 mg/kg, i.p.) and intracardially perfused with freshly prepared 4% paraformaldehyde in 0.1 M phosphate buffer (PB). After perfusion, the bilateral sciatic nerves and fourth lumbar vertebrae (L4) DRGs were quickly removed. All tissues were post-fixed in 4% paraformaldehyde for 4 h and then transferred to 15% sucrose (Nacalai Tesque) solution in 0.1 M PB for 24 h at 4°C. All tissues were then

frozen in embedding compound (Sakura Finetek, Torrance, CA). Frozen sections (16 μm) were cut with a cryostat (Leica CM 1850; Leica Microsystems, Wetzlar, Germany) and thaw-mounted on MAS-coated glass slides (Matsunami Glass, Osaka, Japan). The sections were then blocked in blocking buffer (PBS containing 0.1% Tween 20 and 5% normal goat serum; Vector Laboratories) for 1 h at room temperature and subsequently incubated for 24 h at 4°C with the following primary antibodies: rabbit anti-Iba1 (1:500; Wako Pure Chemical Industries, Osaka, Japan), rat anti-Gr-1/Ly-6G antibody (1:200; R&D Systems) or rat anti-CD31 antibody (1:100; Becton, Dickinson and Company, Franklin Lakes, NJ). The antibodies were washed three times with PBS and incubated for 1.5 h at room temperature with the appropriate secondary antibodies conjugated to Alexa Fluor™ 488 and/or 594 (1:200). The slides were then cover-slipped with Vectashield (Vector Laboratories). All images were acquired using a laser scanning confocal microscope (Fluoview FV10i Confocal Microscope, Olympus, Tokyo, Japan). Next, 6–9 fields (2–3 fields x three independent samples) were selected randomly from each group, and the numbers of immunolabeled cells were counted. An area of each sample section was analyzed using a computer-assisted system (ImageJ software; National Institute of Mental Health, Bethesda, MD). Cell numbers per mm^2 were then calculated.

Primary culture of Schwann cells from the rat sciatic nerves

Primary Schwann cells were harvested from the sciatic nerves of neonatal rats as described previously (40) with minor modifications. Briefly, sciatic nerves were obtained from rat pups (postnatal day 2–3) under sterile conditions. The nerves were washed twice in ice-cold PBS and resuspended in 1 mL culture medium (serum-free Advanced DMEM/F-12, Thermo Fisher Scientific; supplemented with 0.292 mg/mL L-glutamine and 1% penicillin-streptomycin) containing 250 U/mL hyaluronidase type I-S (Sigma-Aldrich) and 160 U/mL collagenase type I (Sigma-Aldrich). After incubating at 37°C for 1 h, the tissue fragments were dissociated by trituration, and the suspension was centrifuged at 300 x g for 5 min at room temperature. After re-suspension in maintenance medium (culture medium containing 2 μM forskolin (Sigma-Aldrich) dissolved in DMSO and supplemented with 13ng/mL heregulin β-1 (Sigma-Aldrich) dissolved in 5% trehalose (Nacalai Tesque),the cells were cultured on poly-L-lysine (PLL; Sigma-Aldrich)-coated 100 mm culture dishes (Corning Incorporated, New York, NY). After 2 days of culture, Schwann cells were purified by magnetic-activated cell separation with a monoclonal antibody against the immature Schwann cell marker p75 neurotrophin receptor (Merck Millipore, Darmstadt, Germany), according to the manufacturer's instructions (Miltenyi Biotec, Bergisch Gladbach, Germany). After 2 days, contaminating fibroblasts were removed by complement-mediated cytolysis using a mouse anti-CD90/Thy1 antibody (Bio-Rad Laboratories, Hercules, CA) and rabbit complement-HLA-ABC (Cappel Laboratories, West Chester, PA). Purified immature Schwann cells were then cultured under standard conditions (in maintenance medium) on tissue culture dishes with 0.1 mg/mL PLL. After 4–7 days, cells were cultured in differentiation medium (serum-free Advanced DMEM/F-12 containing 1% penicillinstreptomycin,0.292 mg/mL L-glutamine, 20 μM forskolin, and

20 ng/mL heregulin β-1) for 2 days on plates (Greiner Bio One International, Kremsm ü nster, Austria) or dishes with 0.1 mg/mL PLL and 0.5 μg/mL laminin (Thermo Fisher Scientific). From 2 days after plating and culture in the differentiation medium, cells were exposed to gp120 or vehicle for 3 days.

Primary culture of rat DRG neurons

DRGs were dissected from embryonic day 15 Wistar/ST rat pups and plated (2 x 10^5 cells per well) in 24-well plates coated with 0.1 mg/mL PLL and 0.5 μg/mL laminin (Thermo Fisher Scientific), and containing Neurobasal medium (Thermo Fisher Scientific) containing 2% B-27 supplement (Thermo Fisher Scientific), 2 mM Lglutamine, 1% penicillin-streptomycin, and 0.05 μg/mL nerve growth factor 2.5S (Sigma-Aldrich). Non-neuronal cells were removed by treating the cultures with medium containing 5-fluorodeoxyuridine (Sigma-Aldrich). Ten days later, the cultures were switched to fresh medium without 5-fluorodeoxyuridine. Purified DRG neuronal cells were further cultured for 10 days on PLL/laminin-coated coverslips in Neurobasal medium.

Cell Migration assay of RAW 264.7 cells

A CytoSelect™ 96-well cell migration assay (8 μm, Fluorometric Format; Cell Biolabs, San Diego, CA) was performed according to manufacturer's instructions. Briefly, the murine macrophage cell line RAW 264.7 was obtained from American Type Culture Collection (TIB-71TM; ATCC, Manassas, VA) and maintained in 100 mm culture dishes containing DMEM (ATCC) supplemented with 10% FBS and 1% penicillin-streptomycin. After 3 days of treating primary cultured DRG neurons and Schwann cells with gp120 IIIB (5 nM), gp120 MN (5 nM), or vehicle (0.1% RSA), the supernatant (conditioned medium) was collected. 150 μL of each conditioned medium or culture medium containing 5 nM X4 gp120 or 1 nM recombinant mouse CXCL1 was added to the bottom chamber. RAW 264.7 cells were then suspended in serum-free DMEM containing 1% penicillin-streptomycin and added to the top membrane chamber. After 24 h incubation at 37°C, the migrating cells were detached from the underside of the membrane by incubation in cell detachment solution at 37°C for 30 min. The dislodged cells were incubated for 20 min at room temperature in CyQuant®GR dye solution diluted in 4 x lysis buffer to be lysed and stained. The fluorescence intensity was then measured using a fluorescence plate reader (Mithras LB940; Berthold Technologies Bioanalytic, Bad Wildbad, Germany) at 480/520 nm.

Immunocytochemical analysis of cultured cells

After treating Schwann cells, DRG neurons, or RAW 264.7 cells with X4 gp120 for 3 days, the culture medium was removed, and the cells were washed with PBS and fixed with 4% paraformaldehyde in PBS for 20 min at room temperature. Cells were washed three times with PBS, blocked, and permeabilized for 30 min in 3% BSA in PBS containing 0.1% Tween 20. Consecutively, the cells were incubated with rat anti-myelin basic protein (MBP; 1:300; Merck Millipore Co., Darmstadt, Germany), rabbit anti-p75 (1:500; Abcam, Cambridge, UK), rat anti-F4/80 (1:200; Santa Cruz Biotechnology,

Dallas, TX), rabbit anti-CXCR4 (1:50; Novus Biologicals, Centennial, CO), or rabbit anti-CCR5 (1:100; Novus Biologicals) primary antibodies overnight at 4°C. After washing three times with PBS, the cells were incubated for 2 h at room temperature with appropriate secondary antibodies conjugated to Alexa Fluor™ 594 and/or Alexa Fluor™ 488 (1:200; Thermo Fisher Scientific). After washing, the cells were mounted using Vectashield containing DAPI (Vector Laboratories, Burlingame, CA), and images were acquired under a laser scanning confocal microscope (Fluoview FV10i Confocal Microscope; Olympus, Tokyo, Japan).

Immunohistochemistry in mouse sciatic nerve and DRG sections

After perineural application of gp120 or vehicle, mice were deeply anesthetized with sodium pentobarbital (50 mg/kg, i.p.) and intracardially perfused with freshly prepared 4% paraformaldehyde in 0.1 M phosphate buffer (PB). After perfusion, the bilateral sciatic nerves and fourth lumbar vertebrae (L4) DRGs were quickly removed. All tissues were post-fixed in 4% paraformaldehyde for 4 h and then transferred to 15% sucrose (Nacalai Tesque) solution in 0.1 M PB for 24 h at 4°C. All tissues were then frozen in embedding compound (Sakura Finetek, Torrance, CA). Frozen sections (16 μm) were cut with a cryostat (Leica CM 1850; Leica Microsystems, Wetzlar, Germany) and thaw-mounted on MAS-coated glass slides (Matsunami Glass, Osaka, Japan). The sections were then blocked in blocking buffer (PBS containing 0.1% Tween 20 and 5% normal goat serum; Vector Laboratories) for 1 h at room temperature and subsequently incubated for 24 h at 4°C with the following primary antibodies: rabbit anti-Iba1 (1:500; Wako Pure Chemical Industries, Osaka, Japan), rat anti-Gr-1/Ly-6G antibody (1:200; R&D Systems) or rat anti-CD31 antibody (1:100; Becton, Dickinson and Company, Franklin Lakes, NJ). The antibodies were washed three times with PBS and incubated for 1.5 h at room temperature with the appropriate secondary antibodies conjugated to Alexa Fluor™ 488 and/or 594 (1:200). The slides were then cover-slipped with Vectashield (Vector Laboratories). All images were acquired using a laser scanning confocal microscope (Fluoview FV10i Confocal Microscope, Olympus, Tokyo, Japan). Next, 6–9 fields (2–3 fields x three independent samples) were selected randomly from each group, and the numbers of immunolabeled cells were counted. An area of each sample section was analyzed using a computer-assisted system (ImageJ software; National Institute of Mental Health, Bethesda, MD). Cell numbers per mm^2 were then calculated.

Reverse transcription-polymerase chain reaction (RT-PCR) assay

Total RNA was extracted from Schwann cells, DRG neurons, and RAW 264.7 cells using an SV Total RNA Isolation system (Promega, Madison, WI) according to the manufacturer's instructions. Purified total RNA was quantified in a spectrophotometer at 260 nm (NanoDrop 2000; Thermo Fisher Scientific). To prepare first strand cDNA, 0.2–1.0 μg RNA was incubated in 40 μL reaction buffer containing a dNTP mixture, RT random primers, and reverse transcriptase (High Capacity cDNA Reverse Transcription Kit; Thermo Fisher Scientific), according to the manufacturer's instructions.

Each target gene was amplified in a 50 μL PCR solution containing 2 mM $MgCl_2$, 0.2 mM dNTP mix, DNA polymerase (Blend Taq®, TOYOBO, Osaka, Japan) and synthesized primers designed according to the GenBank™ sequence as shown in Table 2-1. Samples were sequentially heated to 94°C for 2.5 min, 55°C for 30 sec, and 72°C for 1 min and cycled 30 or 35 times through 94°C for 30 sec, 55°C for 30 sec, and 72°C for 1 min, with a final extension step at 72°C for 3 min.

The mixture was run on 1.5% agarose gel with the indicated markers (TOYOBO). The agarose gel was stained with ethidium bromide (Nacalai Tesque) and photographed under UV transillumination (PhotoDoc-It™ Imaging System, Analytik Jena AG, Jena, Germany).

Quantitative analysis by real-time PCR

Total RNA isolation from Schwann cells and RAW 264.7 were conducted as described above. To extract total RNA from the sciatic nerve, the sciatic nerve was extirpated from gp120- or vehicle-treated mice, and cut 3 mm on either side of the application sites. The sciatic nerve was homogenized with a polytron homogenizer at 19,000 rpm for 1–2 min, and then cDNA was prepared as described above. cDNA was amplified in 20 μL PCR solution containing 10 μL Power SYBR® Green PCR Master Mix (Thermo Fisher Scientific) and in synthesized primers designed according to the GenBank™ sequence, as shown in Table 2-1. PCR was performed using a StepOnePlus™ System (Thermo Fisher Scientific) under the following cycling conditions: 95°C for 10 min and 60°C for 1 min, followed by 40 cycles of 95°C for 15 sec and 60°C for 1 min. Fluorescence was detected after each extension step. *Gapdh* was used as a normalization control, and relative mRNA levels were calculated using a comparative C_t method and StepOnePlus™ software (Thermo Fisher Scientific).

Microarray analysis

After 3 days incubation of primary cultured Schwann cells with vehicle (0.1% RSA) or gp120 (5 nM), total RNA was extracted from three different samples as described above. RNA from each sample was hybridized to RT^2 Profiler PCR arrays according to the manufacturer's protocol (Qiagen, Venlo, the Netherlands). The array was probed according to the manufacturer's instructions in the StepOnePlusTM System (Thermo Fisher Scientific). Gene expression data were analyzed with web-based RT^2 Profiler PCR Array Data Analysis software, which performed ΔΔCt based fold-change calculations from the uploaded threshold cycle data (http://pcrdataanalysis.sabiosciences.com/pcr/arrayanalysis.php?target=upload).

Statistical analysis

Data are presented as means ± S.E.M. and were analyzed using GraphPad Prism version 5.0. (GraphPad Software, San Diego, CA). Differences between two groups were compared using a Student's t-test or Mann–Whitney U-test. Data from more than two groups were compared using a one-way or two-way analysis of variance (ANOVA), followed by a Bonferroni's or Tukey's multiple comparisons test.

Statistical analyses of the 50% withdrawal thresholds in the von Frey filament test were performed using a Mann–Whitney U-test or Kruskal–Wallis test followed by Dunn's multiple comparison test for each day. In all cases, $p < 0.05$ was considered statistically significant.

Table 2-1. Sequences of synthesized primers used in real-time PCR

Synthesized primers used in RT-PCR assay

Target name	Species		Primer sequence	GenBank™ sequence accession number
Cxcr2	Mouse	Sense	5'-CTG AGC CTT GTG GGG AAC TC-3'	NM_009909.3
		Antisense	5'-GCA AGG TCA GGG CAA AGA AC-3'	
Cxcr4	Mouse	Sense	5'-GCT GGC TGA AAA GGC AGT CT-3'	NM_009911.3
		Antisense	5'-TGT CAT CCC CCT GAC TGA TG-3'	
	Rat	Sense	5'-GGC TGA AAA GGC CGT CTA TG-3'	NM_022205
		Antisense	5'-CTG GAA CTG GAA CAC CAC CA-3'	
Ccr5	Mouse	Sense	5'-CCA CAC CCT GTT TCG CTG TA-3'	NM_009917.5
		Antisense	5'-GGT GGT CAG GAG GAG GAC AA-3'	
	Rat	Sense	5'-ACT TGG CTA TTG TCC ATG CT-3'	NM_053960
		Antisense	5'-CCA TGA CAA GTA GGG GTA GG-3'	
Gapdh	Mouse	Sense	5'-GCG AGA CCC CAC TAA CAT CA-3'	GU214026.1
		Antisense	5'-TGG TTC ACA CCC ATC ACA AA-3'	
	Rat	Sense	5'-GTT ACC AGG GCT GCC TTC TC-3'	NM_017008
		Antisense	5'-TGA TGA CCA GCT TCC CAT TC-3'	

Synthesized primers used in real-time PCR assay

Target name	Species		Primer sequence	GenBank™ sequence accession number
Cxcl1	Mouse	Sense	5'-AGA CCA TGG CTG GGA TTC AC -3'	NM_008176.3
		Antisense	5'-AGC TTC AGG GTC AAG GCA AG-3'	
	Rat	Sense	5'-CCC AAA CCG AAG TCA TAG CC-3'	NM_030845.1
		Antisense	5'-TGG GGA CAC CCT TTA GCA TC-3'	
Cd206	Mouse	Sense	5'-TCT TTG CCT TTC CCA GTC TCC-3'	NM_008625.2
		Antisense	5'-TGA CAC CCA GCG GAA TTT C-3'	
Cd86	Mouse	Sense	5'-TTG TGT GTG TTC TGG AAA CGG AG-3'	NM_019388.3
		Antisense	5'-AAC TTA GAG GCT GTG TTG CTG GG-3'	
Il6	Mouse	Sense	5'-GGG ACT GAT GCT GGT GAC AA-3'	NM_001314054.1
		Antisense	5'-TGC CAT TGC ACA ACT CTT TTC T-3'	
Il10	Mouse	Sense	5'-GCA TGG CCC AGA AAT CAA GG-3'	NM_010548.2
		Antisense	5'-GAG AAA TCG ATG ACA GCG CC-3'	
Irf4	Mouse	Sense	5'-GCA GCT CAC TTT GGA TGA CAC-3'	NM_013674.2
		Antisense	5'-TAT GAA CCT GCT GGG CTG GC-3'	
Irf5	Mouse	Sense	5'-CTC TCT GTC CAA AGC TGG CA-3'	NM_001252382.1
		Antisense	5'-ACT ACA TGC CAC ATC CAG GC-3'	
Gapdh	Mouse	Sense	5'-GCG AGA CCC CAC TAA CAT CA-3'	GU214026.1
		Antisense	5'-TGG TTC ACA CCC ATC ACA AA-3'	
	Rat	Sense	5'- GTT ACC AGG GCT GCC TTC TC-3'	NM_017008
		Antisense	5'-TGA TGA CCA GCT TCC CAT TC-3'	

Results

Factors released from Schwann cells in response to X4 gp120 treatment were responsible for macrophage chemoattraction

X4 gp120 strains are known to use CXCR4, but not CCR5, as a principal coreceptor for infection or entry into T-lymphocytes (9,10). Thus, I determined the expression of CXCR4 and CCR5 in the murine macrophage cell line RAW 264.7, primary cultured DRG neurons and Schwann cells. As shown in Fig. 2-1A, both CXCR4- and CCR5-IRs were observed in RAW 264.7 cells and primary cultured DRG neurons, while CXCR4-IR, but not CCR5-IR, was detected in primary cultured Schwann cells. Consistently, the expressions of *Cxcr4* and *Ccr5* mRNA were detected in RAW 264.7 cells and DRG neurons. Schwann cells had little expression of *Ccr5* mRNA, while *Cxcr4* mRNA was detected in these cells (Fig. 2-1B).

Despite robust CXCR4 expression in RAW 264.7 cells, DRG neurons, and Schwann cells, in vitro treatment with gp120 IIIB (5 nM) or MN (5 nM) for 3 days did not change the viability of these cells (Fig. 2-2). Furthermore, I did not detect any meaningful changes in the expression of pro- and anti-inflammatory macrophage-related genes such as *Cd86* (a pro-inflammatory macrophage marker), *Irf5* (a transcription factor involved in pro-inflammatory macrophage polarization), *Cd206* (an anti-inflammatory macrophage marker), and *Irf4* (a transcription factor involved in anti-inflammatory macrophage polarization) in RAW 264.7 cells 3 days after treatment with gp120 IIIB or MN (Fig. 2-3A). Consistent with a previous report (41), treatment with gp120 IIIB (5 nM) or MN (5 nM) for 3 days caused axonal degeneration in MAP-2 positive cultured DRG neurons (Fig. 2-3B). By contrast, treatment with gp120 had no effect on the morphology of Schwann cells, or on the expression of *Mbp* (a differentiated Schwann cell marker) or *p75* (an immature Schwann cell marker) (Fig. 2-3C). To better understand the mechanisms underlying macrophage infiltration into peripheral neurons after X4 gp120 application, I investigated macrophage chemoattraction toward conditioned medium collected from gp120-treated DRG neurons or Schwann cells. Culture medium containing gp120 IIIB (5 nM) or MN (5 nM) did not induce a chemotactic response in RAW 264.7 cells, suggesting that gp120 did not have direct chemotactic effects on macrophages (Fig. 2-3D). I failed to detect macrophage chemotaxis toward the conditioned medium collected from DRG neurons treated with gp120 IIIB (5 nM) or MN (5 nM) for 3 days (Fig. 2-3E). However, RAW 264.7 cells demonstrated significant chemotactic responses toward conditioned medium from Schwann cells treated with either gp120 IIIB or MN (Fig. 2-3F).

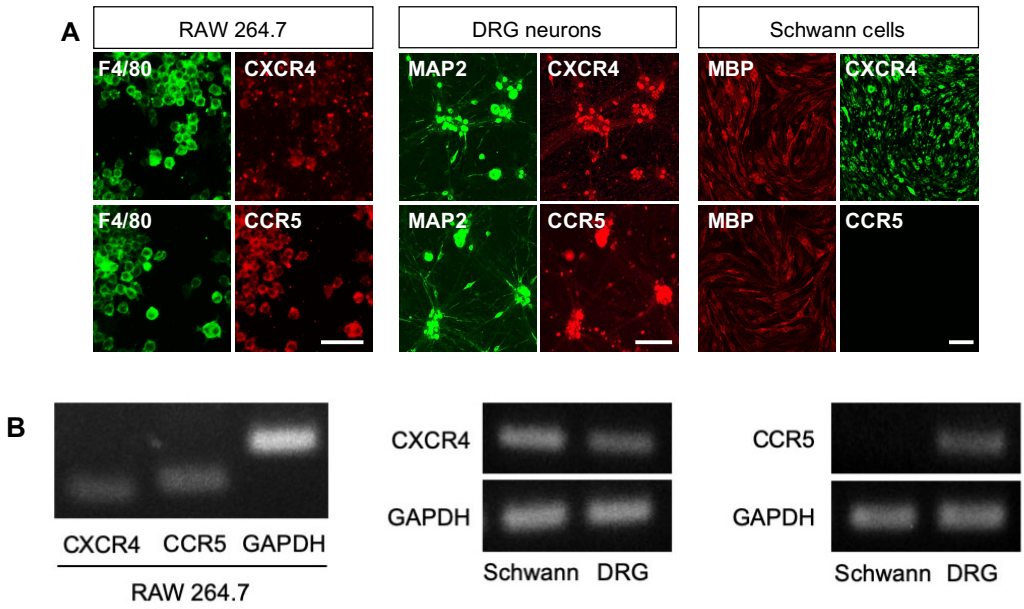

Fig. 2-1. Chemokine receptor expression on macrophages, primary cultured DRG neurons and Schwann cells. (A) Representative confocal microscopy images showing CXCR4- or CCR5-immunoreactivity in RAW 264.7 cells, rat primary cultured dorsal root ganglia (DRG) neurons and rat primary cultured Schwann cells, double stained with anti-F4/80, MAP2 or MBP antibodies, respectively. Scale bar = 100 μm. **(B)** Representative RT-PCR images of Cxcr4 and Ccr5 mRNA expression in RAW 264.7, rat primary cultured Schwann cells, and rat primary cultured DRG neurons. Gapdh is shown as an internal control.

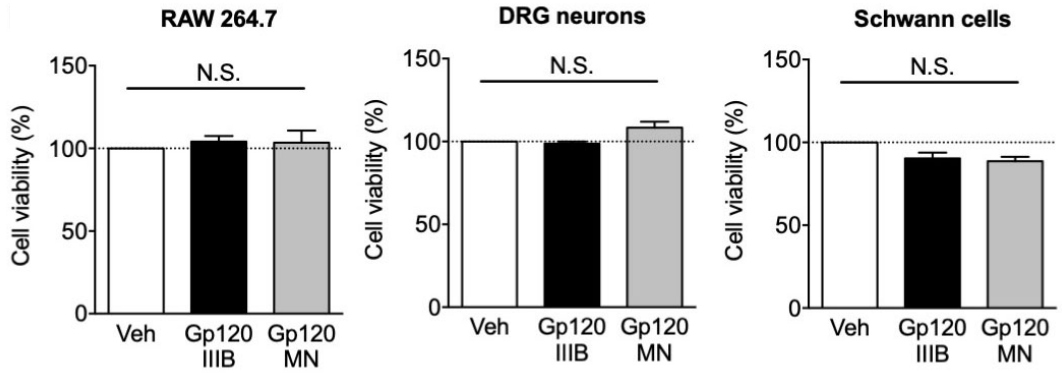

Fig. 2-2. Viability assay. Viability of RAW 264.7, Schwann cells, and DRG neurons 3 days after exposure to gp120 IIIB (5 nM), gp120 MN (5 nM), or vehicle (0.1% RSA). Cell viability was measured using an 3-(4,5-dimethyl-2-thiazolyl)-2,5-diphenyltetrazolium (MTT) assay, and the results were expressed as percentage relative to vehicle-treated cells (dashed lines). Each column represents the mean ± S.E.M. n = 3–6. N.S.: not significant.

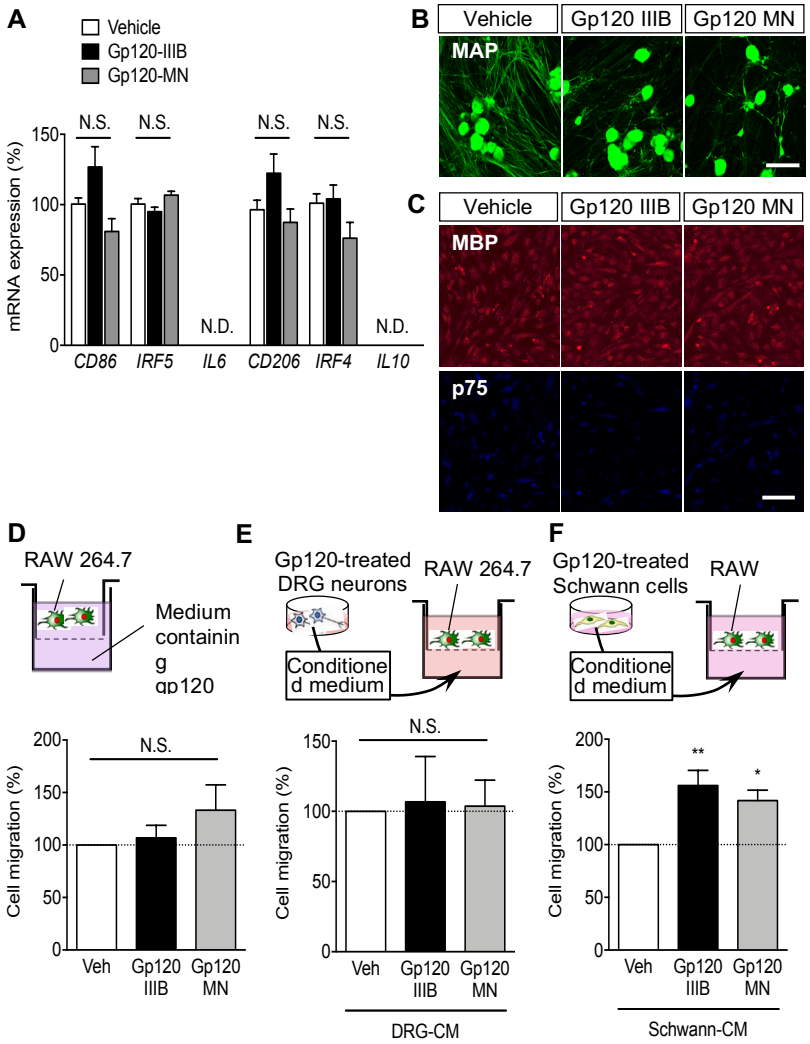

Fig. 2-3. Secreted factors responsible for macrophage chemoattraction in response to X4 gp120 treatment. **(A)** Quantitative real-time PCR analysis of pro- and anti-inflammatory macrophage-related genes such as Cd86, Irf5, Il6, Cd206, Irf4, and Il10 in RAW 264.7 cells after treatment with either gp120 IIIB (5 nM) or MN (5 nM) for 3 days. Each mRNA level was normalized to Gapdh mRNA and expressed relative to the normalized level in the vehicle-treated group. n = 6. N.S.: not significant. N.D.: not detected. **(B)** Immunostaining for MAP2 (green) in cultured DRG neurons and **(C)** double-immunostaining for MBP (red) and p75 (blue) in cultured Schwann cells after treatment with either gp120 IIIB (5 nM) or MN (5 nM) for 3 days. Scale bar =100 μm. (**D–F**) Cell migration assay using RAW 264.7 cells. Cell migrations (%) of RAW 264.7 cells toward culture medium containing gp120 IIIB (5 nM) or MN (5 nM) **(D)**, or conditioned media collected from cultured DRG neurons **(E)** or from cultured Schwann cells (**F**) treated with gp120 IIIB (5 nM) or MN (5 nM) for 3 days. Each value (%) was expressed relative to the data in the vehicle-treated group.n = 3–6. *p < 0.05, ** p < 0.01 vs. vehicle-treated group (Bonferroni's multiple comparisons test following one-way ANOVA). N.S.: not significant. Each column represents the mean ± S.E.M.

Table 2-2. List of genes included in the RT^{2}ProfilerTM PCR Array

GenBank™ accession #	Symbol	Description
NM_144744	Adipoq	Adiponectin, C1Q and collagen domain containing
NM_017178	Bmp2	Bone morphogenetic protein 2
NM_012827	Bmp4	Bone morphogenetic protein 4
NM_013107	Bmp6	Bone morphogenetic protein 6
NM_001191856	Bmp7	Bone morphogenetic protein 7
XM_001079130	C5	Complement component 5
NM_001191092	Ccl1	Chemokine (C-C motif) ligand 1
NM_019205	Ccl11	Chemokine (C-C motif) ligand 11
NM_001105822	Ccl12	Chemokine (C-C motif) ligand 12
NM_057151	Ccl17	Chemokine (C-C motif) ligand 17
NM_001108661	Ccl19	Chemokine (C-C motif) ligand 19
NM_031530	Ccl2	Chemokine (C-C motif) ligand 2
NM_019233	Ccl20	Chemokine (C-C motif) ligand 20
NM_001008513	Ccl21	Chemokine (C-C motif) ligand 21
NM_057203	Ccl22	Chemokine (C-C motif) ligand 22
NM_001013045	Ccl24	Chemokine (C-C motif) ligand 24
NM_013025	Ccl3	Chemokine (C-C motif) ligand 3
NM_053858	Ccl4	Chemokine (C-C motif) ligand 4
NM_031116	Ccl5	Chemokine (C-C motif) ligand 5
NM_001007612	Ccl7	Chemokine (C-C motif) ligand 7
NM_053353	Cd40lg	CD40 ligand
NM_001106878	Cd70	Cd70 molecule
NM_013166	Cntf	Ciliary neurotrophic factor
NM_023981	Csf1	Colony stimulating factor 1 (macrophage)
NM_053852	Csf2	Colony stimulating factor 2 (granulocyte-macrophage)
NM_017104	Csf3	Colony stimulating factor 3 (granulocyte)
NM_017129	Ctf1	Cardiotrophin 1
NM_134455	Cx3cl1	Chemokine (C-X3-C motif) ligand 1
NM_030845	Cxcl1	Chemokine (C-X-C motif) ligand 1
NM_139089	Cxcl10	Chemokine (C-X-C motif) ligand 10
NM_182952	Cxcl11	Chemokine (C-X-C motif) ligand 11
NM_022177	Cxcl12	Chemokine (C-X-C motif) ligand 12
NM_001017496	Cxcl13	Chemokine (C-X-C motif) ligand 13
NM_001017478	Cxcl16	Chemokine (C-X-C motif) ligand 16
NM_138522	Cxcl3	Chemokine (C-X-C motif) ligand 3
NM_145672	Cxcl9	Chemokine (C-X-C motif) ligand 9
NM_012908	Faslg	Fas ligand (TNF superfamily, member 6)
NM_019216	Gdf15	Growth differentiation factor 15
NM_207592	Gpi	Glucose phosphate isomerase
NM_001271218	Ifna2	Interferon alpha 2
NM_138880	Ifng	Interferon gamma
NM_012854	Il10	Interleukin 10
NM_133519	Il11	Interleukin 11
NM_053390	Il12a	Interleukin 12a
NM_022611	Il12b	Interleukin 12b
NM_053828	Il13	Interleukin 13
NM_013129	Il15	Interleukin 15
NM_001105749	Il16	Interleukin 16
NM_001106897	Il17a	Interleukin 17A
NM_001015011	Il17f	Interleukin 17F
NM_019165	Il18	Interleukin 18
NM_017019	Il1a	Interleukin 1 alpha

Table 2-2 (continued).

GenBank™ accession #	Symbol	Description
NM_031512	Il1b	Interleukin 1 beta
NM_022194	Il1rn	Interleukin 1 receptor antagonist
NM_053836	Il2	Interleukin 2
NM_001108943	Il21	Interleukin 21
NM_001191988	Il22	Interleukin 22
NM_130410	Il23a	Interleukin 23, alpha subunit p19
NM_133311	Il24	Interleukin 24
XM_344962	Il27	Interleukin 27
NM_031513	Il3	Interleukin 3
NM_201270	Il4	Interleukin 4
NM_021834	Il5	Interleukin 5
NM_012589	Il6	Interleukin 6
NM_013110	Il7	Interleukin 7
NM_001105747	Il9	Interleukin 9
NM_022196	Lif	Leukemia inhibitory factor
NM_080769	Lta	Lymphotoxin alpha (TNF superfamily, member 1)
NM_212507	Ltb	Lymphotoxin beta (TNF superfamily, member 3)
NM_031051	Mif	Macrophage migration inhibitory factor
NM_019151	Mstn	Myostatin
NM_001106394	Nodal	Nodal homolog (mouse)
NM_001006961	Osm	Oncostatin M
NM_001007729	Pf4	Platelet factor 4
NM_153721	Ppbp	Pro-platelet basic protein (C-X-C motif ligand 7)
NM_012881	Spp1	Secreted phosphoprotein 1
NM_031131	Tgfb2	Transforming growth factor, beta 2
NM_031133	Thpo	Thrombopoietin
NM_012675	Tnf	Tumor necrosis factor (TNF superfamily, member 2)
NM_012870	Tnfrsf11b	Tumor necrosis factor receptor superfamily, member 11b
NM_145681	Tnfsf10	Tumor necrosis factor (ligand) superfamily, member 10
NM_057149	Tnfsf11	Tumor necrosis factor (ligand) superfamily, member 11
NM_031836	Vegfa	Vascular endothelial growth factor A
NM_134361	Xcl1	Chemokine (C motif) ligand 1
NM_031144	Actb	Actin, beta
NM_012512	B2m	Beta-2 microglobulin
NM_012583	Hprt1	Hypoxanthine phosphoribosyltransferase 1
NM_017025	Ldha	Lactate dehydrogenase A
NM_001007604	Rplp1	Ribosomal protein, large, P1

Schwann cell CXCL1 expression was increased by X4 gp120 treatment

Based on the results of the chemotaxis assay, I analyzed alterations in gene expression in primary cultured Schwann cells treated with gp120 IIIB (5 nM) for 3 days using an Inflammatory Cytokines & Receptors RT^2 ProfilerTM PCR Array, with a particular focus on the most commonly implicated genes in inflammation, disease states, and neurotoxicity. Genes included in the RT^2 ProfilerTM PCR Array are shown in Table 2-2. I observed differential expression profiles of cytokines and chemokines between vehicle- and gp120 IIIB-treated Schwann cells (Fig. 2-4A). Among the 89 genes examined, six genes were upregulated in all three samples of gp120 IIIB treated Schwann cells (>2-fold) over the vehicle-treated cells, and five genes were downregulated (>2-fold) (Table 2-3). Expression of genes

encoding ribosomal proteins (*Rpl13a* and *Rplp1*), lactate dehydrogenase A, and the housekeeping protein β-actin (*Actb*) did not differ between vehicle- and gp120-treated groups (data not shown). The six upregulated genes were verified with a real-time PCR assay. Among these genes, I confirmed significant mRNA upregulation of only *Cxcl1* in gp120 IIIB-treated Schwann cells (Fig. 2-4B). In regards to the other five genes, I was unable to detect robust expression in primary cultured Schwann cells, or a meaningful expression difference between vehicle- and gp120 IIIB-treated cells. I next investigated the effect of perineural gp120 IIIB (13 nM) application on the expression of *Cxcl1* mRNA in the mouse sciatic nerve neuroaxis. Consistent with my in vitro findings, *Cxcl1* mRNA was significantly upregulated in the ipsilateral sciatic nerve 7 days after gp120 IIIB application (Fig. 2-4C)

Table 2-3. **Summary of fold changes in gene expression in gp120 IIIB-treated Schwann cells vs. vehicle-treated Schwann cell**

Upregulated genes		Downregulated genes	
Name	Fold-change	Name	Fold-change
Cxcl11	5.53	*Cxcl16*	0.26
Il22	4.56	*Lif*	0.28
Il18	4.20	*Cx₃cl1*	0.32
Il15	2.44	*Tgfβ2*	0.35
Cxcl1	2.28	*Il21*	0.49
Il23 α	2.28		

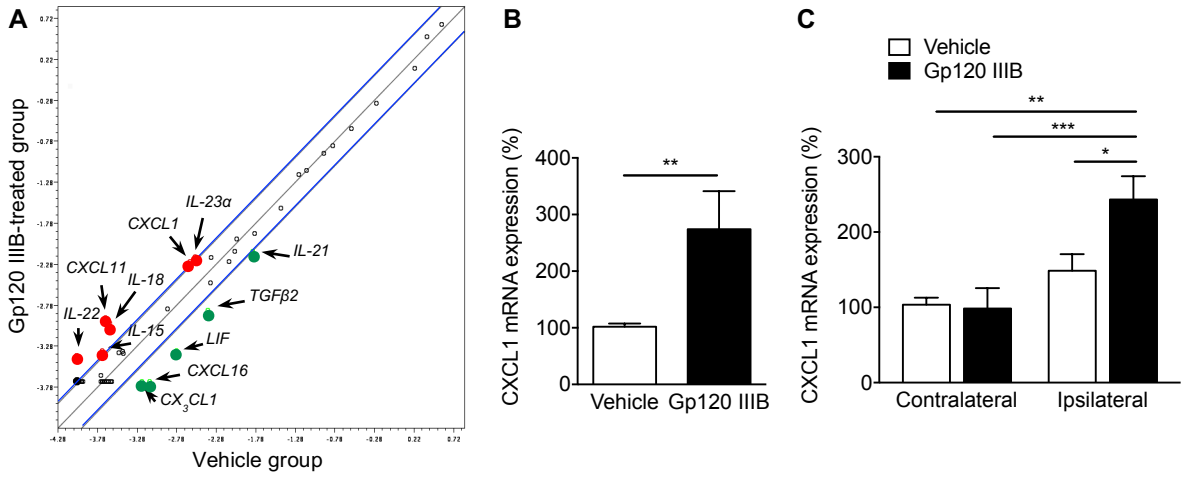

Fig. 2-4. Altered Cxcl1 expression in primary cultured Schwann cells treated with gp120 IIIB. (A) Representative data of gene expression analysis in primary cultured Schwann cells after treatment with vehicle (0.1% RSA) or gp120 IIIB (5 nM) for 3 days. The relative expression levels of each gene (open and colored circles) in vehicle-treated and gp120 IIIB-treated samples were plotted against each other. Red circles: genes with higher expression levels in gp120 IIIB-treated Schwann cells (> 2-fold); green circles: genes with lower expression levels (> 2-fold) in gp120 IIIB-treated Schwann cells; and open circles: no change (≤2-fold). The two blue lines indicate the 2-fold changes from the middle diagonal line. **(B)** Quantitative real-time PCR analysis of Cxcl1 mRNA expression in primary cultured Schwann cells treated with vehicle (0.1% RSA) or gp120 IIIB (5 nM) for 3 days. Each mRNA level was normalized to Gapdh mRNA and expressed relative to the normalized level in the vehicle-treated group. n=10–12. **p < 0.01 (Mann–Whitney U test). **(C)** Quantitative real-time PCR analysis of Cxcl1 mRNA expression in the contralateral or ipsilateral sciatic nerve neuroaxis 7 days after perineural gp120 IIIB application (13 nM). Each mRNA level was normalized to Gapdh mRNA and expressed

relative to the normalized level in the contralateral side of vehicle-treated mice. n = 10. *p < 0.05, **p < 0.01, and ***p < 0.001 (Bonferroni's multiple comparisons test following two-way ANOVA). Each column represents the mean ± S.E.M.

CXCL1 elicited macrophage infiltration and pain behaviors

I next determined whether CXCL1 could directly induce macrophage infiltration into the sciatic nerve and DRG. As shown in Fig. 2-5A , I confirmed mRNA expression of *Cxcr2* (the receptor for CXCL1) in RAW 264.7 cells. The chemotactic response of RAW 264.7 cells toward culture medium containing rCXCL1 (50 nM) was significantly increased compared with vehicle-containing medium (Fig. 2-5B). In mice, perineural application of rCXCL1 (50 nM) to the sciatic nerve induced infiltration of Iba1-positive macrophages into the ipsilateral sciatic nerve and DRG compared with vehicle-treated mice 7 days after application (Fig. 2-5C). Perineural rCXCL1 application also tended to increase neutrophil migration into the sciatic nerve at 3 and 7 days post-application, and into the DRG at 3 days post-application, but neutrophil recruitment was not significant (Fig. 2-6B). Furthermore, perineural rCXCL1 application induced significant mechanical hypersensitivity and spontaneous pain behaviors in the ipsilateral hind paw compared with vehicle-treated mice (Fig. 2-5D–E).

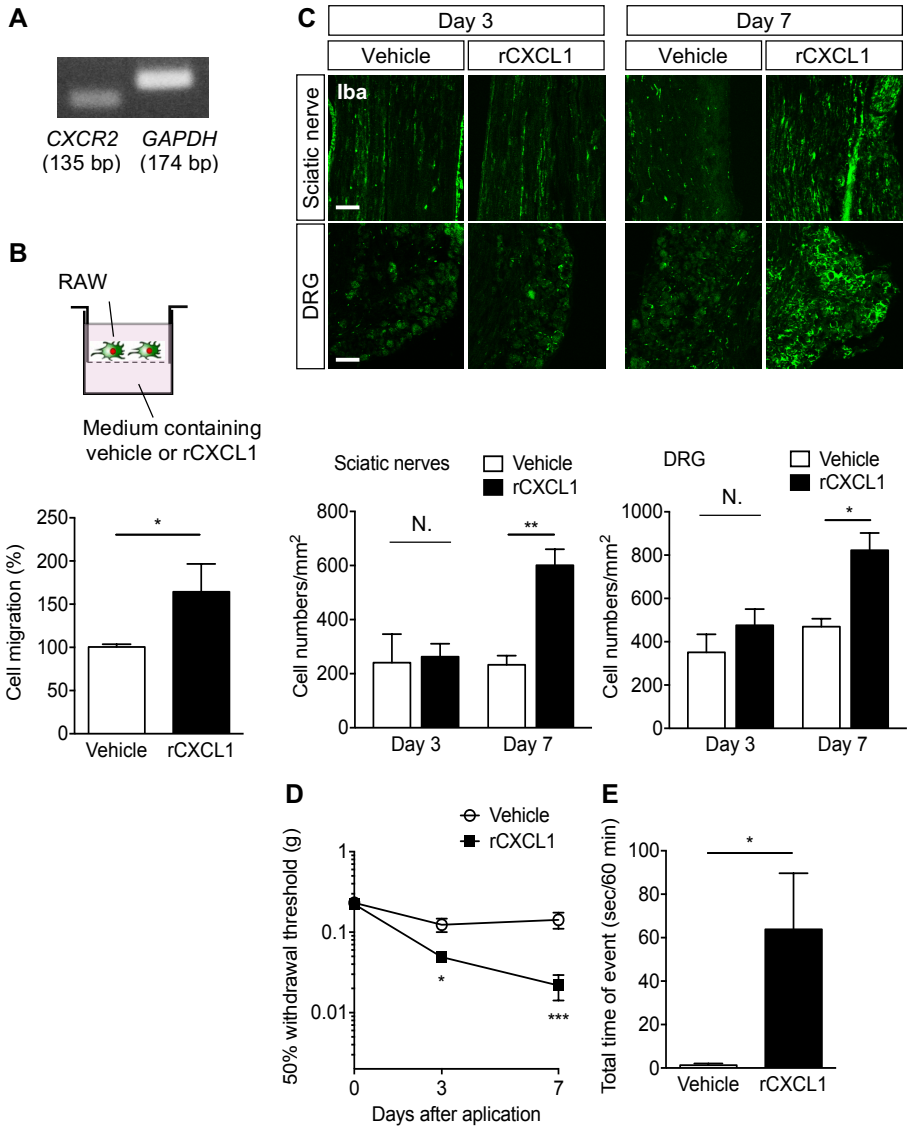

Fig. 2-5. CXCL1-elicited chemotactic response of macrophages and pain-like behavior. (A) Representative RT-PCR images of Cxcr2 mRNA expression in RAW 264.7 cells. Gapdh mRNA was used as an internal control. **(B)** Chemotactic response of RAW 264.7 cells toward rCXCL1 (50 nM)-containing culture medium. The value of cell migration (%) was expressed relative to the data in vehicle-treated cells. n=5. *p < 0.05 (Mann–Whitney U test). (C–E) rCXCL1 (50 nM) or vehicle (0.1% RSA) was perineurally applied to the mouse sciatic nerve. **(C)** The upper panels show representative confocal microscopy images for Iba1-immunoreactivity in the ipsilateral sciatic nerve and dorsal root ganglia (DRG) 3 and 7 days after the application, respectively. Scale bar = 100 μm. The lower graphs show the quantitative analyses for the number of Iba1-labeled cells (macrophages) per mm2. n = 3. *p < 0.05, **p < 0.01 (Bonferroni's multiple comparisons test following two-way ANOVA). N.S.: not significant. **(D)** Time-course changes in 50% withdrawal threshold (g) in response to mechanical stimuli in the ipsilateral hindpaw. Paw withdrawal thresholds were assessed using von Frey filaments just before rCXCL1 application (day 0) and 3 and 7 days after rCXCL1 application. n = 9–10. *p < 0.05, ***p < 0.001 vs. vehicle-treated group (Mann–Whitney U test). **(E)** Total duration (sec) of spontaneous pain-like behaviors (flinching, scratching, and biting/licking) in the ipsilateral hind paw during a 60 min observation period 7 days after rCXCL1 application. n =9–10. * p < 0.05 (Mann–Whitney U test). Each column
or point represents the mean ± S.E.M.

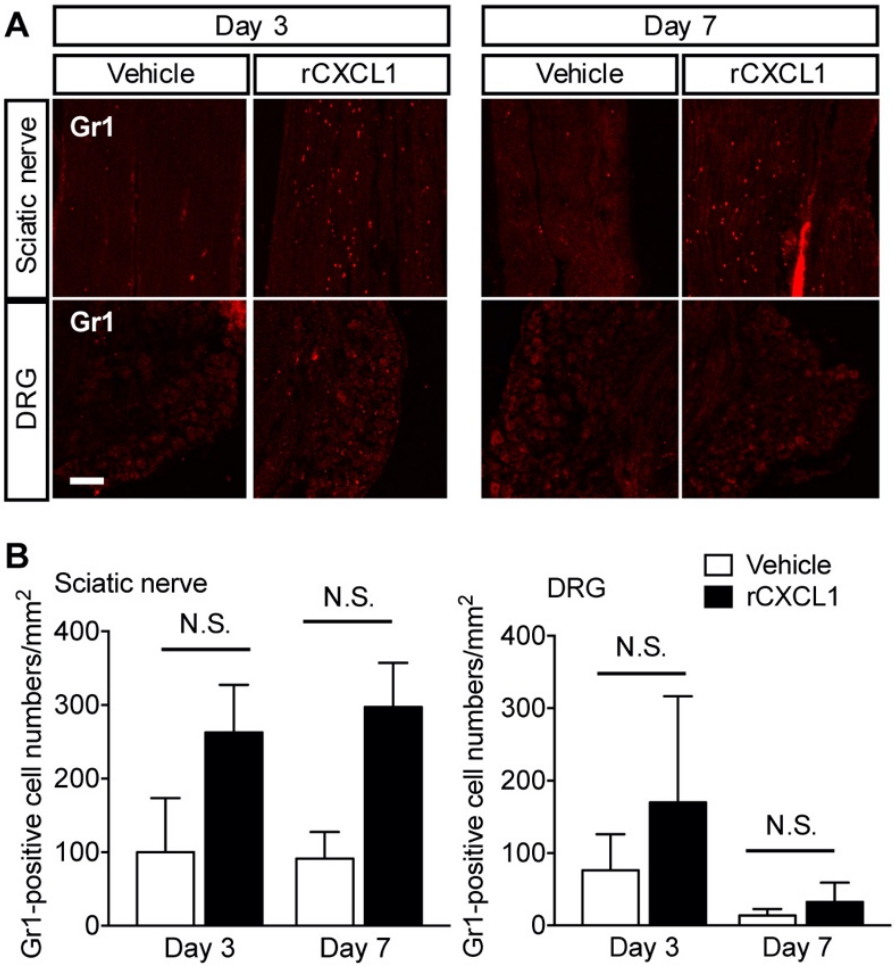

Fig. 2-6. CXCL1-elicited chemotactic response of neutrophils. (A) The upper panels show representative confocal microscopy images for Gr1-immunoreactivity in the ipsilateral sciatic nerve and dorsal root ganglia (DRG) 3 and 7 days after the application, respectively. Scale bar = 100 μm. **(B)** The lower graphs show the quantitative analyses for the number of Gr1-labeled cells (neutrophils) per mm2. N.S: not significant. (Bonferroni's multiple comparisons test following two-way ANOVA).

Inhibition of CXCL1/CXCR2 signaling suppressed gp120-induced macrophage infiltration and pain behaviors

To determine whether CXCL1/CXCR2 signaling between Schwann cells and macrophages contributed to X4 gp120-induced pain behaviors, I examined the effect of a CXCR2 antagonist, SB225002. SB225002 (4 mg/kg) or vehicle control (1% DMSO) was injected intraperitoneally 1 h before, and 2, 4 and 6 days after perineural application of gp120 IIIB (13 nM). SB225002 significantly inhibited gp120 IIIB-induced mechanical hypersensitivity in the ipsilateral hind paw (Fig. 2-7A), as well as macrophage infiltration in the ipsilateral sciatic nerve and DRG 7 days after gp120 application (Fig. 2-7B).

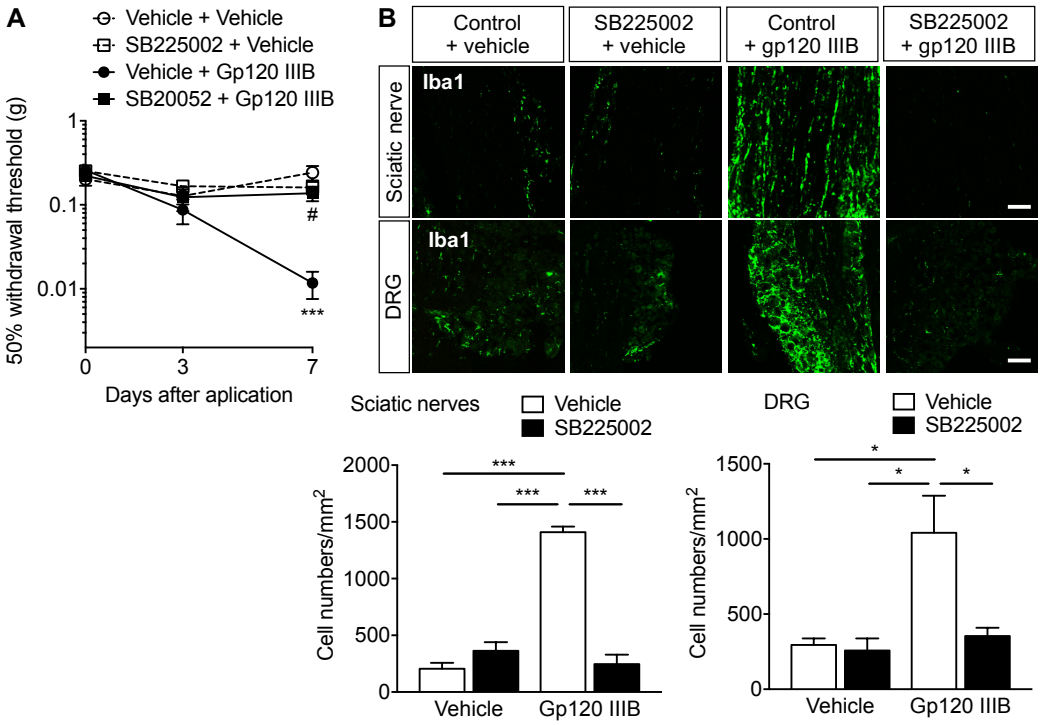

Fig. 2-7. Effects of the CXCR2 antagonist SB220052 on gp120 IIIB-induced mechanical hypersensitivity and macrophage recruitment. SB225002 (4 mg/kg) or vehicle control (1% DMSO) was injected intraperitoneally 1 h before, and 2, 4 and 6 days after perineural gp120 IIIB (13 nM) or vehicle (0.1% RSA) application. **(A)** Time course changes in 50% withdrawal threshold (g) in response to mechanical stimuli in the ipsilateral hindpaw after the gp120 application. Paw withdrawal thresholds were assessed using von Frey filaments just before gp120 application (day 0) and 3 and 7 days after application. n = 8. ***p < 0.001 vs. vehicle (1% DMSO) + vehicle (0.1% RSA). #p < 0.05 vs. vehicle (1% DMSO) + gp120 IIIB (Dunn's multiple comparisons test following a Kruskal–Wallis test on each day). **(B)** The upper panels illustrate representative confocal microscopy images for Iba1-immunoreactivity in the ipsilateral sciatic nerve and DRG 7 days after gp120 IIIB application. Scale bar: 100 μm. The lower graphs show the quantitative analyses for the number of Iba1-labeled cells (macrophages) per mm2. n = 3. *p < 0.05, ***p < 0.001 (Bonferroni's multiple comparisons test following two-way ANOVA). Each column or point represents the mean ± S.E.M.

I further investigated whether the release of endogenous CXCL1 directly contributes to the development of mechanical hypersensitivity and macrophage infiltration induced by gp120 IIIB application. The mice were perineurally applied with gp120 IIIB to the sciatic nerve on day 0, then a CXCL1 neutralizing antibody (10 μg per mouse), IgG2A isotype control (10 μg per mouse) or vehicle (PBS) were injected

into retro-orbital sinus once a day for 4 consecutive days (on day 3–6). These mice were subjected to pain-like behavior and immunohistochemical analysis on day 7. Repeated injection of CXCL1 antibody significantly reversed the decreased pain threshold on the ipsilateral side in gp120 IIIB-treated mice (Fig. 2-8A). In addition, this neutralizing antibody injection almost abolished Iba1-labeled macrophage infiltration into the ipsilateral sciatic nerve and DRG 7 days after perineural application of gp120 IIIB (Fig. 2-8B).

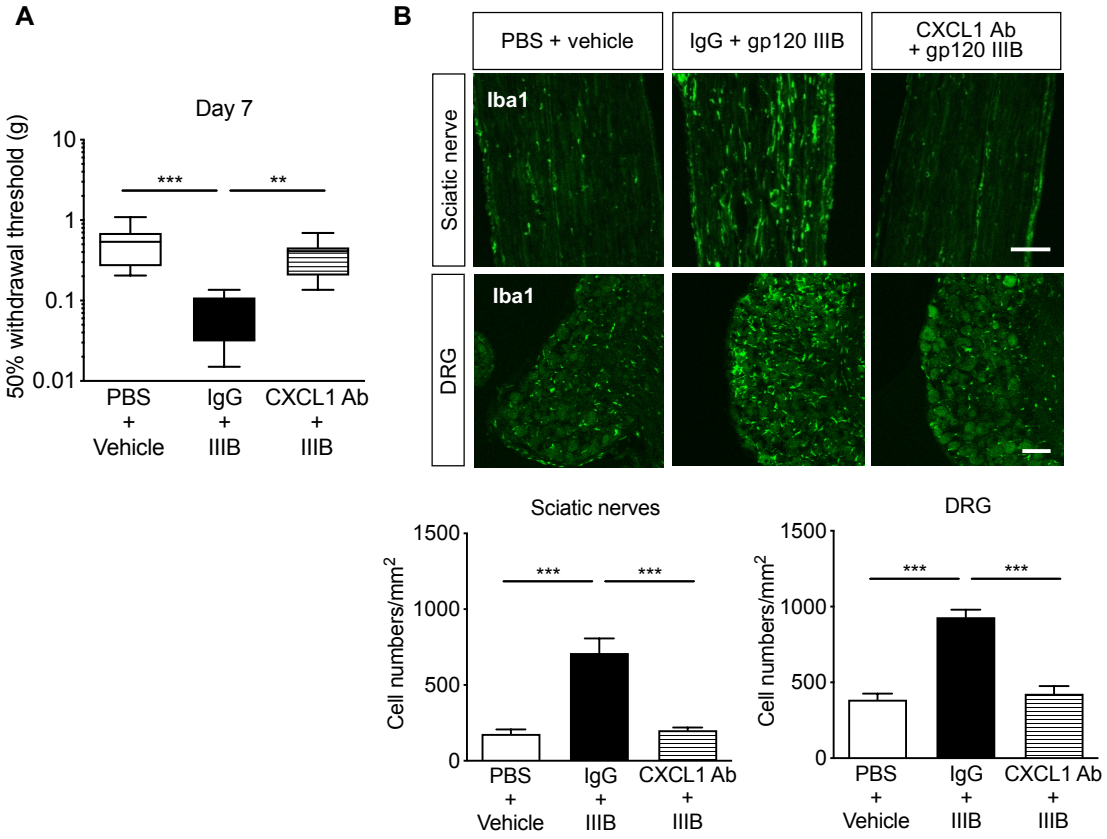

Fig. 2-8. Effects of the CXCL1 neutralizing antibody on gp120 IIIB-induced mechanical hypersensitivity and macrophage recruitment. The mice were perineurally applied with gp120 IIIB (IIIB, 13 nM) or vehicle (0.1% RSA) to the sciatic nerve on day 0, then a CXCL1 neutralizing antibody (CXCL1 Ab, 10 μg per mouse), IgG2A isotype control (IgG, 10 μg per mouse) or PBS were injected into retro-orbital sinus once a day for 4 consecutive days (on day 3–6). **(A)** Changes in 50% withdrawal threshold (g) in response to mechanical stimuli in the ipsilateral hindpaw after the gp120 IIIB application. Paw withdrawal thresholds were assessed using von Frey filaments just before gp120 IIIB application (day 0) and 7 days after application. n=9–10. **p < 0.01, ***p < 0.001 (Dunn's multiple comparisons test following a Kruskal–Wallis test on each day). **(B)** The upper panels illustrate representative confocal microscopy images for Iba1-immunoreactivity in the ipsilateral sciatic nerve and DRG 7 days after gp120 IIIB application. Scale bar = 100 μm. The lower graphs show the quantitative analyses for the number of Iba1-labeled cells (macrophages) per mm2. n = 4. ***p < 0.001 (Bonferroni's multiple comparisons test following one-way ANOVA). Each column represents the mean ± S.E.M.

Discussion

In chapter one, I demonstrated the functional role of macrophage-mediated neuroinflammation in the HIV DSN pathogenesis by using X4 gp120-induced neuropathic pain mouse model. However, this

raised an important question as to the mechanisms underlying X4 gp120-induced infiltration of macrophages. The studies carried out in chapter two have aimed to develop and optimize in vitro and in vivo protocols to allow me to investigate more precisely the key regulators of X4 gp120-induced macrophage infiltration into the peripheral nerves.

R5 HIV-1 gp120 directly induces macrophage migration and facilitates pro-inflammatory cytokine production in macrophages via CCR5 (12,21,42). On the other hand, although macrophages can support the replication of X4 HIV-1 (43), the resultant X4 HIV-1 virus particles cannot directly infect macrophages expressing CXCR4 to elicit their pathogenetic effects (9,20). In the present study, I confirmed a considerable expression of both CXCR4 and CCR5 in the murine macrophage cell line RAW 264.7. However, treatment with X4 gp120 had no effect on cell viability or polarization of RAW 264.7 cells into pro-/anti-inflammatory phenotypes characterized by cytokine and transcription factor productions. Notably, this macrophage cell line exhibited no chemotactic responses toward X4 gp120, suggesting the lack of a direct effect of X4 gp120 on macrophages, consistent with a previous report (42).

Schwann cells not only provide neurotrophic support for sensory nerves to maintain normal function (44,45), but they also contribute to pathogenesis of neuropathic pain by releasing pro-inflammatory factors to recruit immune cells or directly affect sensory neurons (46). An earlier study documented that application of gp120 to the sciatic nerve increases CCL5 (also known as RANTES) production in Schwann cells via CXCR4. CCL5 derived from Schwann cells facilitates TNFα production in DRG neurons, thereby causing TNFα-dependent axonal retraction in an autocrine fashion (41). In the present study, I demonstrated that exposure of cultured Schwann cells to X4 gp120 did not affect cell viability, morphology, or differentiation state (as indicated by consistent expression of MBP), despite expression of CXCR4 on these cells. However, RAW 264.7 cells exhibited chemotactic responses toward conditioned medium from X4 gp120-treated Schwann cells, indicating that Schwann cell-derived soluble factors may recruit macrophages in response to X4 gp120 exposure. I also detected increased CXCL1 expression in both gp120 IIIB-treated primary cultured Schwann cells and in the sciatic nerve neuroaxis (containing abundant myelin-forming Schwann cells) of gp120-treated mice.

Because CXCL1 is known to elicit its biological effects through CXCR2 expressed on macrophages/monocytes, neutrophils, and mast cells (47), I deduced that this chemokine was a Schwann cell-derived macrophage chemoattractant upregulated in response to X4 gp120 exposure. A previous study demonstrated that CXCL1 is produced locally and released in the DRG after nerve injury, and induces neuropathic pain via macrophage and neutrophil infiltration, or by acting directly on primary sensory neurons (48). Consistently, I found that RAW 264.7 cells, which express CXCR2, were chemoattracted to CXCL1. Furthermore, perineural application of CXCL1 elicited mechanical hypersensitivity and spontaneous pain-like behaviors, accompanied by macrophage infiltration. Contrastingly, blockade of CXCR2 with the antagonist SB225002 prevented X4 gp120-induced

macrophage infiltration and pain behaviors. Taken together, the present findings suggest that CXCL1 derived from myelin-forming Schwann cells is responsible for macrophage infiltration into the peripheral nerves in response to X4 gp120 exposure, and therefore may be associated with the development of X4 gp120-induced pain behaviors. However, topical administration of X4 p120 or rCXCL1 to the sciatic nerve increased, but not significantly, Gr1-positive neutrophils in the peripheral nerves. Neutrophil accumulation at the site of nerve injury plays a critical role in neuroinflammation leading to pain, which is modulated by neutrophil secretion of inflammatory substances or induction of monocyte recruitment to the injured site (49). Thus, the involvement of neutrophils in X4 gp120-induced pain behavior and macrophage infiltration cannot be fully ruled out and should be examined in further studies.

Analysis of nerve biopsies from HIV-infected patients has identified degeneration of both myelinated and unmyelinated axons on the peripheral nerves (50). It is also reported that CXCR4 expressed on neurons directly regulates gp120-induced neural cell death via activation of p38 mitogen-activated protein kinase (51). Thus, these pathological changes in sensory neurons have been considered to be one of major causes of HIV DSN. Consistent with these reports, I found in the present study that in vitro treatment with X4 gp120 decreased neuroaxis of primary cultured rat DRG. However, I failed to detect a chemotactic response of RAW 264.7 cells toward the conditioned medium from X4 gp120-treated primary cultured DRG neurons, suggesting that DRG neurons may not be required for macrophage infiltration induced by X4 gp120 exposure. The present study does not exclude the importance of the direct actions of HIV gp120 on peripheral nerves in HIV DSN pathogenesis.

In conclusion, the data presented herein suggests that, interactions between Schwann cells and macrophages via the CXCL1/CXCR2 signaling axis may be responsible in part for enhanced pain signals and development of hypersensitivity in HIV DSN, in conjunction with direct effects by X4 gp120 on peripheral neurons.

Summary

In this study, I investigated the mechanism underlying HIV DSN pathogenesis and newly uncovered a Schwann cell-mediated pathway. My study findings build on already existing literature and also newly brings to light the following findings.

Chapter 1

I show that recombinant X4 HIV-1 gp120 delivered directly to the mouse sciatic nerve induced mechanical hypersensitivity that persisted for weeks. I also newly demonstrate the presence of consistent spontaneous pain-like behaviors in the HIV DSN mouse model rarely reported in other animal models of HIV DSN. Furthermore, through the deletion of macrophages using clodronate liposomes, I clearly demonstrate that the infiltration of macrophages into the peripheral nerves is associated with the development of X4 gp120-induced pain-like behaviors. Taken together, my findings suggest that a macrophage-dependent immune-mediated response may be one of the causal factors of the pathogenesis of X4 gp120-related HIV DSN.

Chapter 2

I identified the key regulators responsible for macrophage infiltration into the peripheral nerve that results in pain-like behaviors. I newly found out that, rather than having a direct chemotactic effect on macrophages, X4 gp120 through its interaction with CXCR4 receptors expressed on Schwann cells induced the upregulation and release of CXCL1 from these cells. I further show that CXCL1/CXCR2 signaling between Schwann cells and macrophages is most likely the cause of macrophage infiltration into the peripheral nerve and resultant pain-like behaviors.

Overall, the data presented herein suggests that the pathogenesis of HIV DSN most likely involves multiple complex pathways, including Schwann cells surrounding the neural axon in sensory nerves. I demonstrated for the first time that X4 gp120 induces release of CXCL1 from Schwann cells to recruit macrophages. These macrophages ultimately converged on neurons to induce hypersensitivity to innocuous stimuli and spontaneous pain behaviors. Although these findings should be expanded in further molecular experiments, I propose that cell-to-cell communication between Schwann cells and macrophages via CXCL1/CXCR2 may be essential for X4 gp120-induced HIV DSN (Summary Figure).

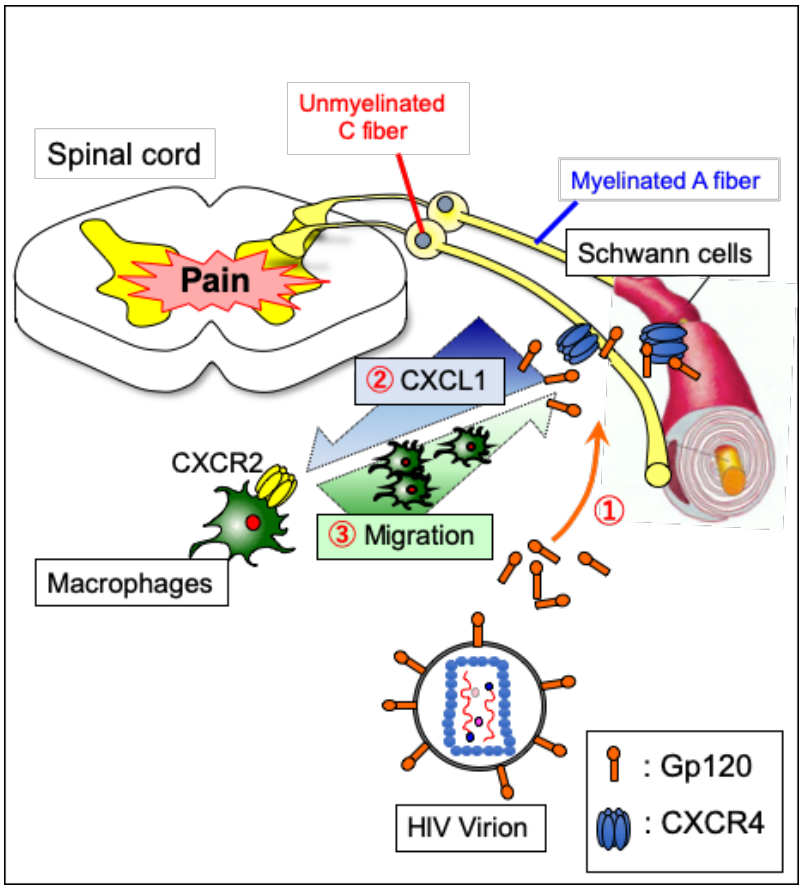

Summary Figure. Proposed mechanism of X4 HIV-1 gp120 induced macrophage infiltration and associate pain-like behaviors. (1) X4 gp120 initially interacts with CXCR4 chemokine receptors express on Schwann cells surrounding the neural axon in sensory nerves.**(2)** In response to X4 gp120 treatment, Schwann cells upregulate and release CXCL1 to chemoattract bone marrow stem cell-derived macrophages through CXCR2 expressed on these cells. **(3)**. These macrophages eventually converge on the neuron to induce mechanical hypersensitivity and spontaneous pain-like behaviors.

Acknowledgements

First and foremost, I would like to express my deepest gratitude to Professor Kazuo Matsubara (Department of Clinical Pharmacology and Therapeutics, Kyoto University Hospital) for giving me an opportunity to conduct this research in his laboratory. The experience and research knowledge that I have gained from working in his lab has been hugely beneficial to me and is sure to open many doors that lie ahead in the next step of my career.

I also wish to express my sincere gratitude to Dr. Takayuki Nakagawa and Dr. Satoshi Imai (Department of Clinical Pharmacology and Therapeutics, Kyoto University Hospital) for their direct guidance in conducting research and for their unwavering commitment which led to publication of our works in a prestigious journal. Dr. Takayuki Nakagawa and Dr. Satoshi Imai have allowed me to gain insight, not only in the understanding of the scientific basis of HIV-related pain, but also in various other types of neuropathic pain. Furthermore, I am very grateful to both of them for always finding the time to discuss the project and resolve any issues that emerged even when they were busy.

I would also like to thank Dr. Atsushi Yonezawa, Dr. Shunsaku Nakagawa, Mr. Kotaro Itohara (Department of Clinical Pharmacology and Therapeutics, Kyoto University Hospital), Dr. Tomohiro Omura (Department of Pharmacy, Kobe University hospital) and Dr. Yuki Sato (Department of Pharmacokinetics, Faculty of Pharmaceutical Sciences, Hokkaido University) for their roles as secondary supervisors and for their many useful advice.

My sincere gratitude also goes out to my colleagues Ms. Ren Hiraiwa, Ms. Madoka Koyanagi, Ms. Mayuna Matsumoto and Dr. Takashi Ogihara who participated greatly in this research to make it the success that it is today. I will of course acknowledge everyone in the Department of Clinical Pharmacology and Therapeutics, Kyoto University Hospital who have all been fantastic people to work with and made the experience even more worthwhile.

Lastly I would like to deeply thank Ms. Sae Maeda, Dr. Kensuke Morris and my entire family who continuously supported me and believed that I could complete my studies in Japan.

List of Publications

Schwann cell-derived CXCL1 contributes to human immunodeficiency virus type 1 gp120-induced neuropathic pain by modulating macrophage infiltration in mice.

Mpumelelo Ntogwa, Satoshi Imai, Ren Hiraiwa, Madoka Koyanagi, Mayuna Matsumoto, Takashi Ogihara, Shunsaku Nakagawa, Tomohiro Omura, Atsushi Yonezawa, Takayuki Nakagawa, Kazuo Matsubara.

Brain Behavior and Immunity. August 2020, Volume 88, Issue 2, pp 325-339.

doi: 10.1016/j.bbi.2020.03.027

References

1. Schutz, S.G., Robinson-Papp, J., 2013. HIV-related neuropathy: current perspectives. HIV AIDS (Auckl) 5, 243–251.
2. Pardo, C.A., McArthur, J.C., Griffin, J.W., 2001. HIV neuropathy: insights in the pathology of HIV peripheral nerve disease. J. Peripher. Nerv. Syst. 6, 21–27.
3. Phillips, T.J., Cherry, C.L., Cox, S., Marshall, S.J., Rice, A.S., 2010. Pharmacological treatment of painful HIV-associated sensory neuropathy: a systematic review and meta-analysis of randomised controlled trials. PLoS One 5, e14433.
4. Brannagan 3rd, T.H., Nuovo, G.J., Hays, A.P., Latov, N., 1997. Human immunodeficiency virus infection of dorsal root ganglion neurons detected by polymerase chain reaction in situ hybridization. Ann. Neurol. 42, 368–372.
5. Jones, G., Zhu, Y., Silva, C., Tsutsui, S., Pardo, C.A., Keppler, O.T., McArthur, J.C., Power, C., 2005. Peripheral nerve-derived HIV-1 is predominantly CCR5-dependent and causes neuronal degeneration and neuroinflammation. Virology 334, 178–193.
6. Peudenier, S., Hery, C., Ng, K.H., Tardieu, M., 1991. HIV receptors within the brain: a study of CD4 and MHC-II on human neurons, astrocytes and microglial cells. Res. Virol. 142, 145–149.
7. Melli, G., Keswani, S.C., Fischer, A., Chen, W., Hoke, A., 2006. Spatially distinct and functionally independent mechanisms of axonal degeneration in a model of HIV-associated sensory neuropathy. Brain 129, 1330–1338.
8. Oh, S.B., Tran, P.B., Gillard, S.E., Hurley, R.W., Hammond, D.L., Miller, R.J., 2001. Chemokines and glycoprotein120 produce pain hypersensitivity by directly exciting primary nociceptive neurons. J. Neurosci. 21, 5027–5035.
9. Littman, D.R., 1998. Chemokine receptors: keys to AIDS pathogenesis? Cell 93, 677–680.
10. Naif, H.M., 2013. Pathogenesis of HIV infection. Infect Dis Rep 5, e6.
11. Naif, H.M., Li, S., Alali, M., Sloane, A., Wu, L., Kelly, M., Lynch, G., Lloyd, A.,Cunningham, A.L., 1998. CCR5 expression correlates with susceptibility of maturing monocytes to human immunodeficiency virus type 1 infection. J. Virol. 72, 830–836.
12. Moss, P.J., Huang, W., Dawes, J., Okuse, K., McMahon, S.B., Rice, A.S., 2015. Macrophage-sensory neuronal interaction in HIV-1 gp120-induced neurotoxicitydouble dagger. Br. J. Anaesth. 114, 499–508.
13. Wallace, V.C., Blackbeard, J., Pheby, T., Segerdahl, A.R., Davies, M., Hasnie, F., Hall, S., McMahon, S.B., Rice, A.S., 2007. Pharmacological, behavioural and mechanistic analysis of HIV-1 gp120 induced painful neuropathy. Pain 133, 47–63.
14. Chattopadhyay, S., Myers, R.R., Janes, J., Shubayev, V., 2007. Cytokine regulation of MMP-9 in peripheral glia: implications for pathological processes and pain in injured nerve. Brain Behav. Immun. 21, 561–568.

15. Martini, R., Fischer, S., Lopez-Vales, R., David, S., 2008. Interactions between Schwann cells and macrophages in injury and inherited demyelinating disease. Glia 56, 1566–1577.
16. Hesselgesser J, Halks-Miller M, DelVecchio V, Peiper SC, Hoxie J, Kolson DL, Taub D, Horuk R (1997) CD4-independent association between HIV-1 gp120 and CXCR4: functional chemokine receptors are expressed in human neurons. Curr Biol 7:112-121.
17. Broder CC, Collman RG (1997) Chemokine receptors and HIV. J Leukoc Biol. 62:20-29.
18. Yuan, S.B., Shi, Y., Chen, J., Zhou, X., Li, G., Gelman, B.B., Lisinicchia, J.G., Carlton, S.M., Ferguson, M.R., Tan, A., Sarna, S.K., Tang, S.J., 2014. Gp120 in the pathogenesis of human immunodeficiency virus-associated pain. Ann. Neurol. 75, 837–850.
19. Bradley, W.G., Shapshak, P., Delgado, S., Nagano, I., Stewart, R., Rocha, B., 1998. Morphometric analysis of the peripheral neuropathy of AIDS. Muscle Nerve 21, 1188–1195.
20. Hahn, K., Robinson, B., Anderson, C., Li, W., Pardo, C.A., Morgello, S., Simpson, D., Nath, A., 2008. Differential effects of HIV infected macrophages on dorsal root ganglia neurons and axons. Exp. Neurol. 210, 30–40.
21. Hao, S., 2013. The molecular and pharmacological mechanisms of HIV-related neuropathic pain. Curr. Neuropharmacol. 11, 499–512.
22. Zheng, W., Ouyang, H., Zheng, X., Liu, S., Mata, M., Fink, D.J., Hao, S., 2011. Glial TNFα in the spinal cord regulates neuropathic pain induced by HIV gp120 application in rats. Mol. Pain 7, 40.
23. Teodorof, C., Divakar, S., Soontornniyomkij, B., Achim, C.L., Kaul, M., Singh, K.K., 2014. Intracellular mannose binding lectin mediates subcellular trafficking of HIV-1 gp120 in neurons. Neurobiol. Dis. 69, 54–64.
24. Callahan, B.L., Gil, A.S., Levesque, A., Mogil, J.S., 2008. Modulation of mechanical and thermal nociceptive sensitivity in the laboratory mouse by behavioral state. J. Pain 9, 174–184.
25. Chaplan, S.R., Bach, F.W., Pogrel, J.W., Chung, J.M., Yaksh, T.L., 1994. Quantitative assessment of tactile allodynia in the rat paw. J. Neurosci. Methods 53, 55–63.
26. Mogil, J.S., Crager, S.E., 2004. What should we be measuring in behavioral studies of chronic pain in animals? Pain 112, 12–15.
27. Brok, H.P., Vossen, J.M., Heidt, P.J., 1998. IFN-γ-mediated prevention of graft-versus host disease: pharmacodynamic studies and influence on proliferative capacity of chimeric spleen cells. Bone Marrow Transplant. 22, 1005–1010.
28. Isami, K., Haraguchi, K., So, K., Asakura, K., Shirakawa, H., Mori, Y., Nakagawa, T., Kaneko, S., 2013. Involvement of TRPM2 in peripheral nerve injury-induced infiltration of peripheral immune cells into the spinal cord in mouse neuropathic pain model. PLoS One 8, e66410.
29. Isami, K., Imai, S., Sukeishi, A., Nagayasu, K., Shirakawa, H., Nakagawa, T., Kaneko, S., 2018. The impact of mouse strain-specific spatial and temporal immune responses on the progression of neuropathic pain. Brain Behav. Immun. 74, 121–132.

30. Herzberg, U., Sagen, J., 2001. Peripheral nerve exposure to HIV viral envelope protein gp120 induces neuropathic pain and spinal gliosis. J. Neuroimmunol. 116, 29–39.
31. Van Rooijen, N., Sanders, A., 1994. Liposome mediated depletion of macrophages: mechanism of action, preparation of liposomes and applications. J. Immunol. Methods 174, 83–93.
32. Yuan, S.B., Ji, G., Li, B., Andersson, T., Neugebauer, V., Tang, S.J., 2015. A Wnt5a signaling pathway in the pathogenesis of HIV-1 gp120-induced pain. Pain 156, 1311–1319.
33. McArthur JC, Sipos E, Cornblath DR, Welch D, Chupp M, Griffin DE, Johnson RT (1989) Identification of mononuclear cells in CSF of patients with HIV infection. Neurology 39:66-70.
34. Griffin JWCT, McArthur JC (1998) Peripheral neuropathies associated with HIV infection. In: The Neurology of AIDS (Gendelman HELS, Epstein L, Swindells S, eds), pp 275-291. New York: Chapman & Hall.
35. Yoshioka, M., Shapshak, P., Srivastava, A.K., Stewart, R.V., Nelson, S.J., Bradley, W.G., Berger, J.R., Rhodes, R.H., Sun, N.C., Nakamura, S., 1994. Expression of HIV-1 and interleukin-6 in lumbosacral dorsal root ganglia of patients with AIDS. Neurology 44, 1120–1130.
36. Nagano, I., Shapshak, P., Yoshioka, M., Xin, K., Nakamura, S., Bradley, W.G., 1996. Increased NADPH-diaphorase reactivity and cytokine expression in dorsal root ganglia in acquired immunodeficiency syndrome. J. Neurol. Sci. 136, 117–128.
37. Ren, K., Dubner, R., 2010. Interactions between the immune and nervous systems in pain. Nat. Med. 16, 1267–1276.
38. Freedman BD, Liu QH, Del CM, Collman RG (2003) HIV-1 gp120 chemokine receptor-mediated signaling in human macrophages. Immunol Res 27:261-276.
39. Klasse PJ, Moore JP (2004) Is there enough gp120 in the body fluids of HIV-1-infected individuals to have biologically significant effects? Virology 323:1-8.
40. Imai, S., Koyanagi, M., Azimi, Z., Nakazato, Y., Matsumoto, M., Ogihara, T., Yonezawa, A., Omura, T., Nakagawa, S., Wakatsuki, S., Araki, T., Kaneko, S., Nakagawa, T., Matsubara, K., 2017. Taxanes and platinum derivatives impair Schwann cells via distinct mechanisms. Sci. Rep. 7, 5947.
41. Keswani, S.C., Polley, M., Pardo, C.A., Griffin, J.W., McArthur, J.C., Hoke, A., 2003. Schwann cell chemokine receptors mediate HIV-1 gp120 toxicity to sensory neurons. Ann. Neurol. 54, 287–296.
42. Lin, C.L., Sewell, A.K., Gao, G.F., Whelan, K.T., Phillips, R.E., Austyn, J.M., 2000. Macrophage-tropic HIV induces and exploits dendritic cell chemotaxis. J. Exp. Med. 192, 587–594.
43. Simmons, G., Reeves, J.D., McKnight, A., Dejucq, N., Hibbitts, S., Power, C.A., Aarons, E., Schols, D., De Clercq, E., Proudfoot, A.E., Clapham, P.R., 1998. CXCR4 as a functional coreceptor for human immunodeficiency virus type 1 infection of primary macrophages. J. Virol. 72, 8453–8457.

44. Chen, Z.L., Yu, W.M., Strickland, S., 2007. Peripheral regeneration. Ann. Rev. Neurosci. 30, 209–233.
45. Hoke, A., 2006. Neuroprotection in the peripheral nervous system: rationale for more effective therapies. Arch. Neurol. 63, 1681–1685.
46. Rutkowski, J.L., Tuite, G.F., Lincoln, P.M., Boyer, P.J., Tennekoon, G.I., Kunkel, S.L., 1999. Signals for proinflammatory cytokine secretion by human Schwann cells. J. Neuroimmunol. 101, 47–60.
47. Olson, T.S., Ley, K., 2002. Chemokines and chemokine receptors in leukocyte trafficking. Am. J. Physiol. Regul. Integr. Comp. Physiol. 283, R7–R28.
48. Silva, R.L., Lopes, A.H., Guimaraes, R.M., Cunha, T.M., 2017. CXCL1/CXCR2 signaling in pathological pain: role in peripheral and central sensitization. Neurobiol. Dis. 105, 109–116.
49. Kiguchi, N., Kobayashi, D., Saika, F., Matsuzaki, S., Kishioka, S., 2017. Pharmacological regulation of neuropathic pain driven by inflammatory macrophages. Int. J. Mol. Sci. 18, E2296.
50. Martin, C., Solders, G., Sonnerborg, A., Hansson, P., 2003. Painful and non-painful neuropathy in HIV-infected patients: an analysis of somatosensory nerve function. Eur. J. Pain 7, 23–31.
51. Kaul, M., Ma, Q., Medders, K.E., Desai, M.K., Lipton, S.A., 2007. HIV-1 coreceptors CCR5 and CXCR4 both mediate neuronal cell death but CCR5 paradoxically can also contribute to protection. Cell Death Differ. 14, 296–305.